Quarterly Research Performance Progress Report

Federal Agency and Organization Element to Which Report is Submitted	U.S. Department of Energy Office of Fossil Energy
FOA Name	Advanced Technology Solutions for Unconventional Oil & Gas Development
FOA Number	DE-FOA-0001722
Nature of the Report	Research Performance Progress Report (RPPR)
Award Number	DE-FE0031606
Award Type	Cooperative Agreement
Name, Title, Email Address, and Phone Number for the Prime Recipient	**Technical Contact (Principal Investigator):** Abhijit Dandekar, Professor, adandekar@alaska.edu 907-474-6427 **Business Contact:** Rosemary Madnick Executive Director UAF Office of Grants and Contracts Administration rmadnick@alaska.edu, 907-474-6446
Name of Submitting Official, Title, Email Address, and Phone Number	Same as PI
Prime Recipient Name and Address	University of Alaska Fairbanks Grants and Contracts Administration PO Box 757880, Fairbanks AK 99775
Prime Recipient Type	Not for profit organization
Project Title	**FIRST EVER FIELD PILOT ON ALASKA'S NORTH SLOPE TO VALIDATE THE USE OF POLYMER FLOODS FOR HEAVY OIL EOR a.k.a ALASKA NORTH SLOPE FIELD LABORATORY (ANSFL)**

Principal Investigator(s)	**PI:** Abhijit Dandekar, *University of Alaska Fairbanks* **Co-PIs:** Yin Zhang, *University of Alaska Fairbanks* John Barnes and Samson Ning, Hilcorp Alaska LLC Randy Seright, *New Mexico Institute* *of Mining & Technology* Baojun Bai, *Missouri University of Science and Technology* Dongmei Wang, *University of North Dakota*
Prime Recipient's DUNS number	615245164
Date of the Report	December 30, 2018
Period Covered by the Report	September 1, 2018 – November 30, 2018
Reporting Frequency	Quarterly
Signature of Principal Investigator:	Abhijit Dandekar

University of Alaska Fairbanks

TABLE OF CONTENTS

LIST OF FIGURES

LIST OF TABLES

LIST OF ACRONYMS

bpd   Barrel per day
cP   Centipoise
gc   Critical gas
MW   Molecular weight
og   Gas-oil
ow   Oil-water
PV   Pore Volume
rg   Gas relative
ro   Oil relative
rog   Oil relative to gas

row	Oil relative to water
rw	Water relative
wi	Irreducible water
XRF	X-ray Fluorescence

1. ACCOMPLISHMENTS

a. Project Goals

The overall objective of this project is to perform a research field experiment to validate the use of polymer floods for heavy oil Enhanced Oil Recovery (EOR) on Alaska North Slope.

The main scientific/technical objectives of the proposed project are:
1. Determine the synergy effect of the integrated EOR technology of polymer, low salinity water, horizontal wells, and conformance treatments (e.g., gels), and its potential to economically enhance heavy oil recovery.
2. Assess polymer injectivity into the Schrader Bluff formations for various polymers at various concentrations.
3. Assess and improve injection conformance along horizontal wellbore and reservoir sweep between horizontal injectors and producers.
4. Evaluate the water salinity effect on the performance of polymer flooding and gel treatments.
5. Optimize pump schedule of low-salinity water and polymer.
6. Establish timing of polymer breakthrough in Schrader Bluff N-sands.
7. Screen an optimized method to control the conformance of polymer flooding at the various stages of the polymer flooding project.
8. Estimate polymer retention from field data and compare with laboratory and simulation results.
9. Assess incremental oil recovery vs. polymer injected.
10. Assess effect of polymer production on surface facilities and remediation methods.

The technical tasks proposed in these studies will focus on the following: (1) optimization of injected polymer viscosity/concentration and quantification of polymer retention via laboratory scale experiments; (2) optimization of injection water salinity and identification of contingencies for premature polymer breakthrough via laboratory scale experiments and numerical analyses; (3) reservoir simulation studies for optimization of polymer injection strategy; (4) design and implementation of a field pilot test at Milne Point on ANS; (5) identification of effective ways to treat produced water that contains polymer, and finally (6) the feasibility of commercial application of the piloted method in ANS heavy oil reservoirs. The project milestones, and current milestone status are shown in **Table 8**.

b. Accomplishments

The primary focus of the research program, in the early stages, has been the initiation of the polymer injection in the already set aside injection wells J-23A and J-24A respectively. In order to complement

the polymer injection, focus of other supporting tasks has been advancing reservoir simulation, tackling flow assurance challenges and laboratory corefloods. The accomplishments to date are summarized in the following bullet points:

- An abstract based on the project submitted for the 2019 SPE Western Region Meeting has been accepted. The paper will be presented in April 2019 in San Jose, CA.[]
- Although, there were some setbacks in the polymer injection such as the presence of hydrocarbon gas in the water that was used to prepare the polymer solution and breakdown of the positive displacement pumps used for injection (due to higher rates), for the most part polymer injection has continued as planned. Water cut has started to decrease in the project producers and no polymer breakthrough has been detected.
- Reservoir simulation task has advanced quite well with a waterflood history matched model.
- Preliminary results on polymer retention have been obtained.
- Salinity effects on residual oil saturation correspond to literature and expectations, based on the preliminary corefloods with commercial core materials.

Since the official project start date of June 1, 2018, the entire project team has been conducting working meetings every other Friday for two hours to discuss the various tasks and the project as a whole. Additionally, separate meetings between the sub-groups, especially reservoir simulation also take place.

The following summarizes the team's progress to date in relation to the various tasks and sub-tasks outlined in the Project Management Plan (PMP):

- Task 1.0 - Project Management and Planning

  PMP and DMP: Activity has been completed, per the dates shown in the first quarterly report.

- Task 2.0 - Laboratory Experiments for Optimization of Injected Polymer Viscosity/Concentration and Quantification of Polymer Retention

Two measurements of polymer retention were made at New Mexico Tech using Milne Point reservoir core material labelled AK-36890, T-19, 3908.2. Both experiments injected a polymer solution containing 1750-ppm SNF Flopaam 3630 HPAM (viscosity was 40.7 cp at $7.3s^{-1}$, 25°C) in synthetic Milne Point Injection brine. This brine contained 0.25% NaCl, 0.185% KCl, 0.073% $CaCl_2$-$2H_2O$, and 0.125% $MgCl_2$-$6H_2O$. In both experiments, sand was packed in a metal tube that was 61 cm (2 ft) long and 0.9 cm in inside diameter. No overburden pressure was applied in either case. Experiments were performed at room temperature (23°C).

In the first experiment, sand was dug out of a consolidated core to produce a loose sand. This sand was naturally coated with a viscous oil. 50.41 grams of this sand was packed into the first tube. Then, two liters (102 pore volumes, PV) of synthetic Milne Point Injection brine were flushed through the sand pack at 8000 cm^3/hr to (9900 ft/d) insure that a residual oil saturation was reached. The sandpack had a pore

volume of 19.58 cm^3, a porosity of 0.409 and a permeability to water of 11.3 Darcys. Next, 11 PV of polymer solution were injected at 29.7 ft/d Darcy velocity. This brine contained 40-ppm KI as a water tracer. Pressure drops across the core were monitored. Effluent samples from the core were collected every 4 cm^3 and subsequently analyzed for tracer concentration (Spectronic Genesys 2 spectrophotometer at 290 nm), effluent viscosity (ProRheo LS-300 viscometer), and carbon and nitrogen. (Shimadzu TOC-L). Carbon and nitrogen are part of the HPAM molecular structure, and so are used to detect the presence and concentration of the polymer in the effluent. A component of the oil (possibly an aromatic ring structure) partitioned into the water phase during the flood and interfered with detection of the KI tracer at 290 nm. Consequently, the tracer could not be reliably analyzed for this particular coreflood. Further, the organic material that partitioned into the water phase was also detected by our total organic carbon analyzer—revealing about 300-ppm of the organic contaminant in the produced brine.

Figure 1 plots values observed during polymer injection into the first Milne Point sand pack. **Figure 2** plots the same effluent data, normalized relative to either the injected concentrations (in the case of viscosity and nitrogen) or to final produced effluent concentrations or values (in the case of carbon and pressure drop across the core). Analysis of this data revealed that some permanent loss of viscosity (8%) resulted from the polymer solution passing through the core—probably due to oxidative degradation. Calculations based on nitrogen analysis of the effluent suggested a polymer retention value of 290 µg/g (µg of polymer retained per gram of rock contacted). If valid, this value would result in a 63% retardation of the polymer bank as it propagated through the reservoir.

As a first step toward understanding the underlying cause of this high retention number, a second experiment was performed where the oil-coated sand was extracted with toluene to remove the oil. Another retention experiment was performed using the same methodology as described above, but using the cleaned sand. The second sand pack had a pore volume of 17.71 cm^3, a porosity of 0.37, a permeability to water of 6.33 Darcys, and contained 57.81 grams of sand. **Figures 3 and 4** show results from this second experiment. Analysis of this data revealed roughly a 5% loss of viscosity from the polymer solution passing through the core. Calculations based on nitrogen analysis of the effluent suggested a polymer retention value of 153 µg/g—corresponding to a 39% delay or retardation factor. Some aspects of this experiment suggested that residual toluene (from the extraction) interfered with the tracer. So, a third experiment will be performed next where the sand will be further cleaned with methanol. We will also attempt to analyze the sand using XRF and particle-sizing.
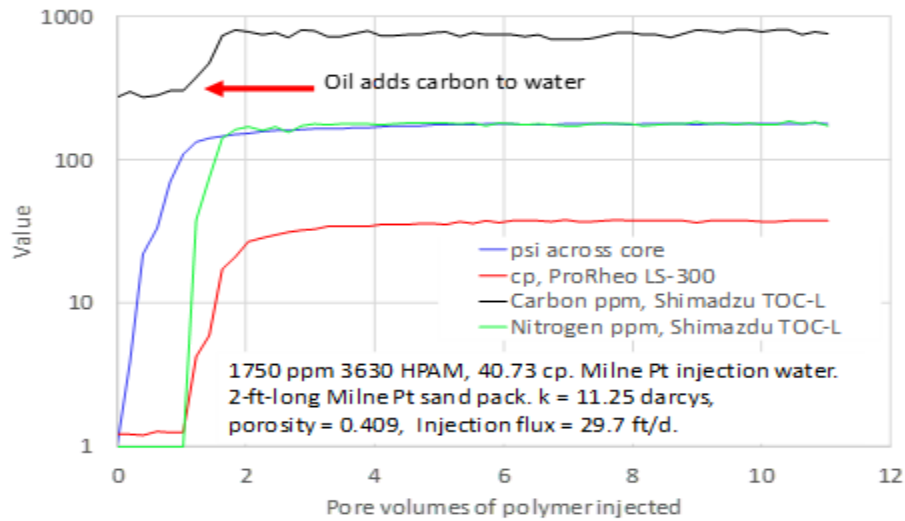
Figure 1 Experimental values during polymer injection for the first Milne Point sandpack.
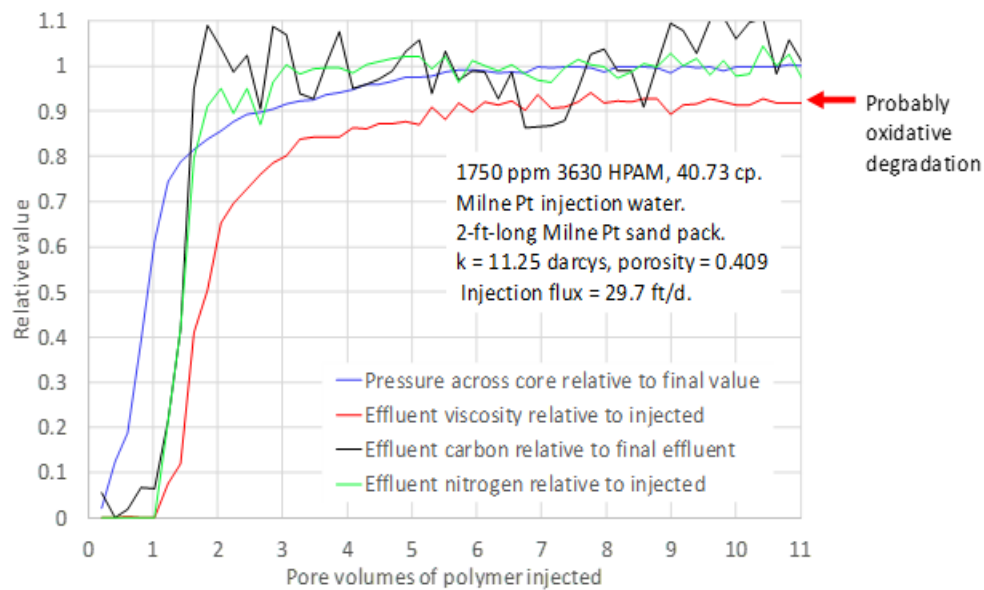
Figure 2 Experimental values from Figure 1, re-plotted as normalized values.
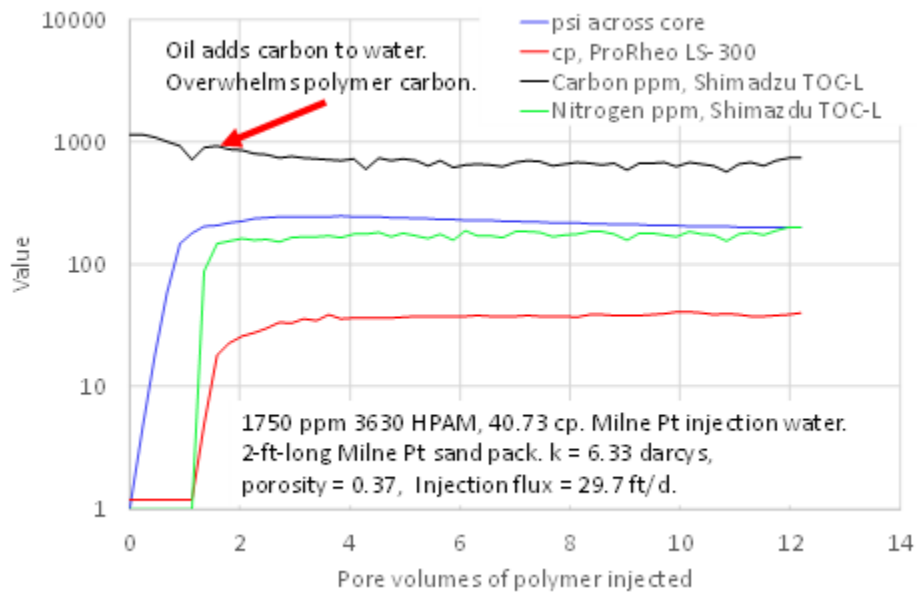
Figure 3 Experimental values during injection for the second retention experiment.
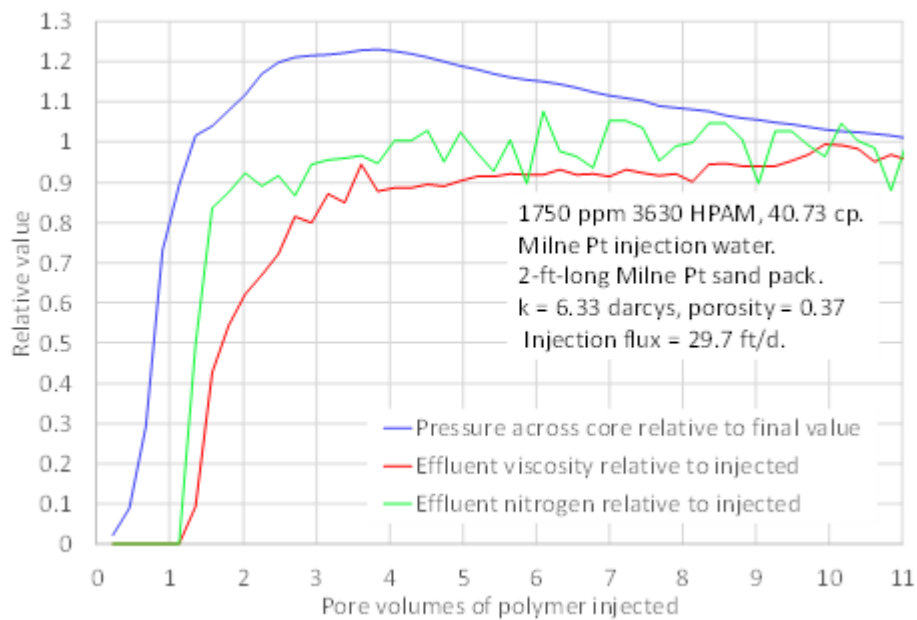
Figure 4 Experimental values during injection for the second retention experiment, re-plotted as normalized values.

Activity is ongoing.

- Task 3.0 - Laboratory Experiments for Optimization of Injection Water Salinity and Identification of Contingencies in Premature Polymer Breakthrough in the Field

The objective of this task in this quarter is to investigate the effect of water salinity on residual oil saturation, which will provide essential basis for the optimization of injection water salinity during polymer flooding. During this quarter, the following progress was achieved.

- Reviewed the mechanisms of low salinity water (LowSal). [*Note that LoSal^{TM} is a trademark of BP*];
- Measured the viscosity of crude oil and the effect of temperature and shear rate on viscosity;
- Measured the viscosity of polymer solution;
- Ran a couple of core flooding experiments to understand the effect of salinity on residual oil saturation using sandpacks.

Review of LowSal EOR Mechanisms

Various mechanisms of LowSal have been reported, including wettability alteration; osmosis; clay (fines) movement; alkaline flooding behavior as a result of increased pH; salting-in effect which means an increased solubility as a result of reduced salinity; multicomponent ion exchange (MIE) effect; and pH change effect. **Table 1** provides additional explanation about these mechanisms. The LowSal can result in local pressure and phase permeability change, interfacial tension (IFT) reduction, and wettability alteration. Consequently, the residual oil saturation and oil recovery factor will change accordingly.

Table 1 Reviewed mechanisms of LowSal.

Type	Mechanism	Explanation	Reference
Pressure/ permeability	Osmosis	Clay distributed at different salinities produces additional pressure, which increases water drive.	Buckley, 2009
	Clay particle (fines) movement	Due to the expansion of the electrical double layers (which may also be ion exchange), clay particles and other mixed wet fines are removed from the rock surface, leaving a water-wet point in low salinity conditions. The penalty for migration may block the narrow pore throat and cause microscopic transfer of the injected water.	Tang, 1999

IFT reduction	Alkaline flooding behavior	pH rises in low-salinity floods high enough to make certain components of oil saponified. This reduces the interfacial tension between water and oil (similar to alkaline flooding). And oil like surfactant flooding.	Buckley, 2009
	"Salting-in" effect	Charged oil components on clay surface are easier to decompose and dissolve in water phase. The salt effect. Loose particles reduce the interfacial tension between water and oil, like a surfactant flood.	Austad, 2008
Wettability change	Multicomponent Ion Exchange (MIE)	Due to expansion of the electric double layer and cation exchange capacity of the clay complex, bound charged organic components of the oil are substituted by Ca^{2+} leading to an increase in the water wetness of the formation.	Lager, 2006; Ligthelm, 2009
	pH driven	The cation exchange capacity of the clays is triggered by near surface pH changes brought about by protons substituting Ca^{2+} on the clay surfaces in low salinity water flooding.	Austad, 2010

Rheological Behavior of Milne Point Crude Oil

The viscosities of the two crude oil samples, B-28 wellhead oil and L-47 wellhead oil, were measured at various shear rates and temperatures (including the reservoir temperature, ~70.5 °F). Both B-28 and L-47 oil samples were provided by Hilcorp from the project wells in Milne Point. The viscosities of the crude oils were measured with HAAKE MARS Rheometer (Thermo Scientific). The sample is put in the space between rotor and the cup and the rotor can rotate at controlled speed. It will shear the sample around it. The shear rate can be changed by changing the rotating speed of the rotor. Therefore, the shear rate is a measure of the speed for the rotor shearing the fluid.

The results are given in the **Figures 5-6**. The results indicate that the B-28 oil has a relatively lower viscosity and shows Newtonian fluid behavior when the shear rate is above 2 s^{-1}. However, the crude oil shows shear-thinning behavior at lower shear rate. As the temperature increases, the viscosity decreases. There is a relatively good linear relationship between the viscosity and temperature in the semi-log plot, as shown in **Figure 7**. The viscosity of L-47 crude oil is shown in **Figures 8-10**. The L-47 crude oil has a much higher viscosity than the B-28 crude oil. It shows shear-thinning behavior when the shear rate is below 10 s^{-1}. Above that, the oil behaves as a Newtonian fluid. The viscosity drastically decreases as the temperature increases, following a relatively linear fashion in the semi-log plot, as shown in **Figure 10**.
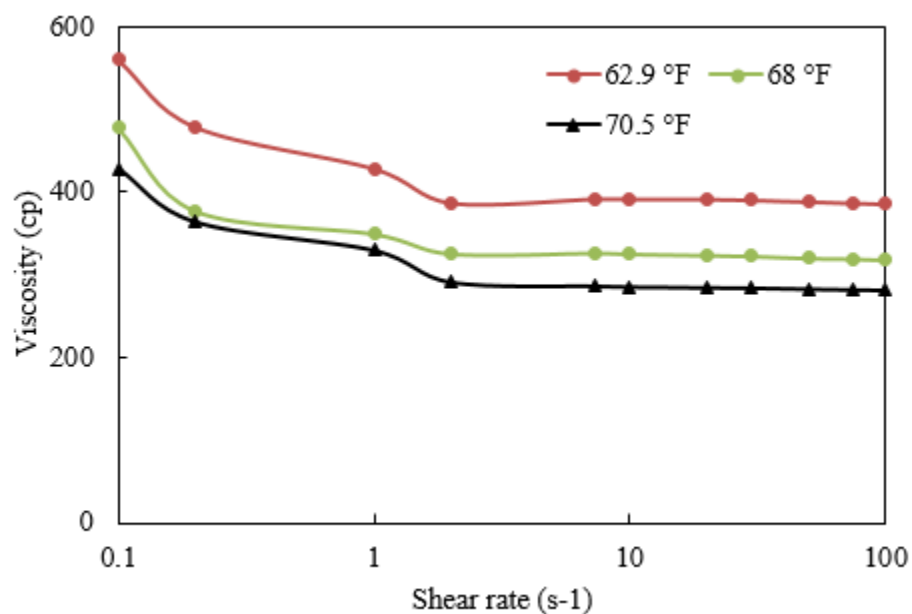
Figure 5 Viscosity of B-28 crude oil at different shear rates (62.9-70.5°F).
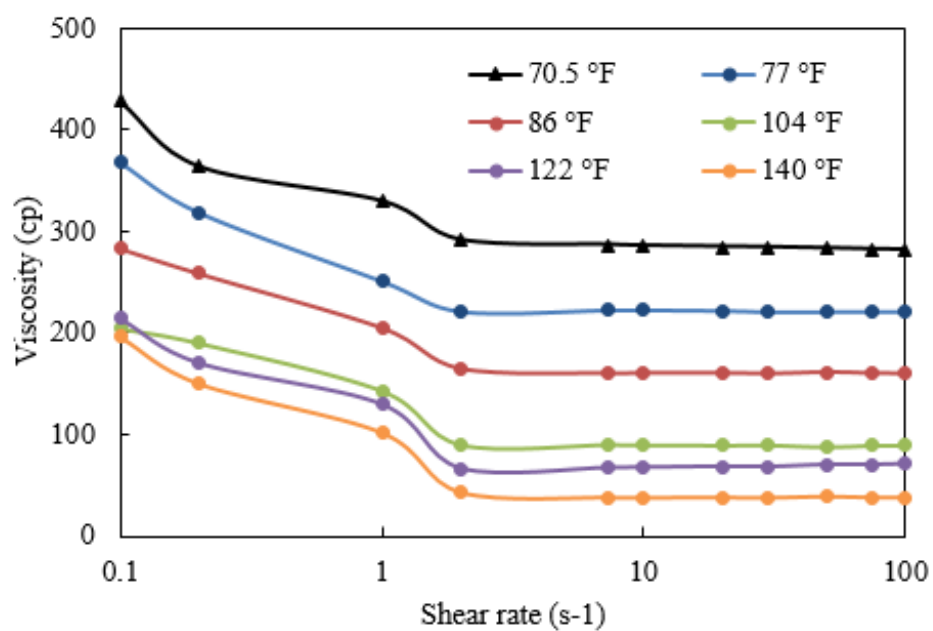
Figure 6 Viscosity of B-28 crude oil at different shear rates (70.5-140°F).
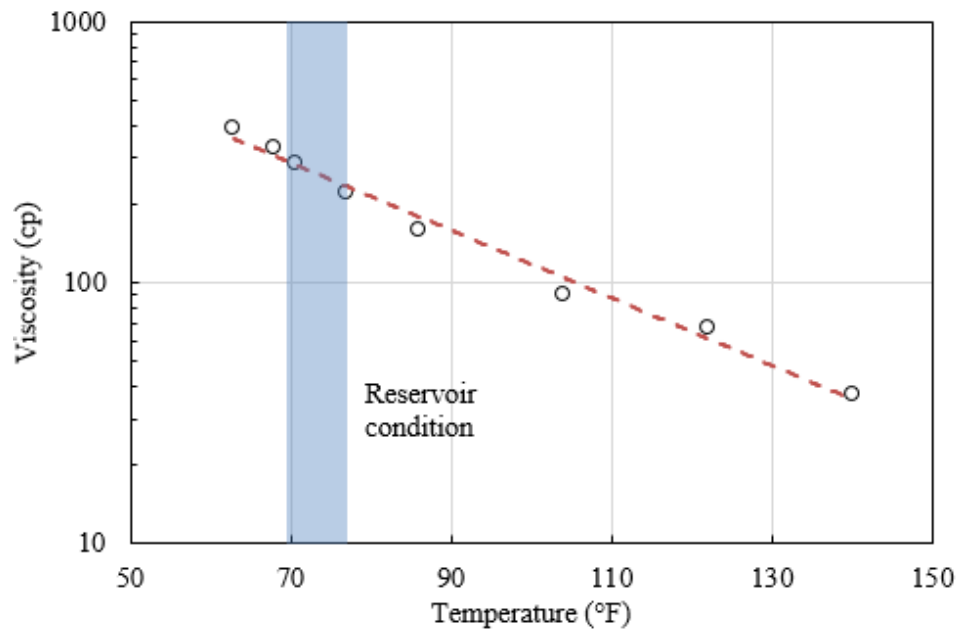
Figure 7 Viscosity of B-28 crude oil at different temperatures.
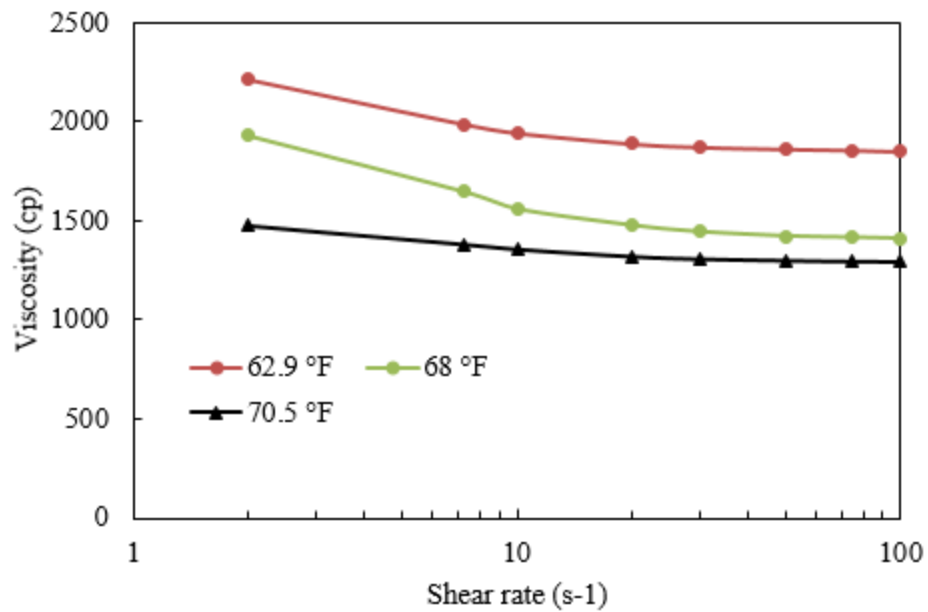
Figure 8 Viscosity of L-47 crude oil at different shear rates (62.9-70.5ºF).
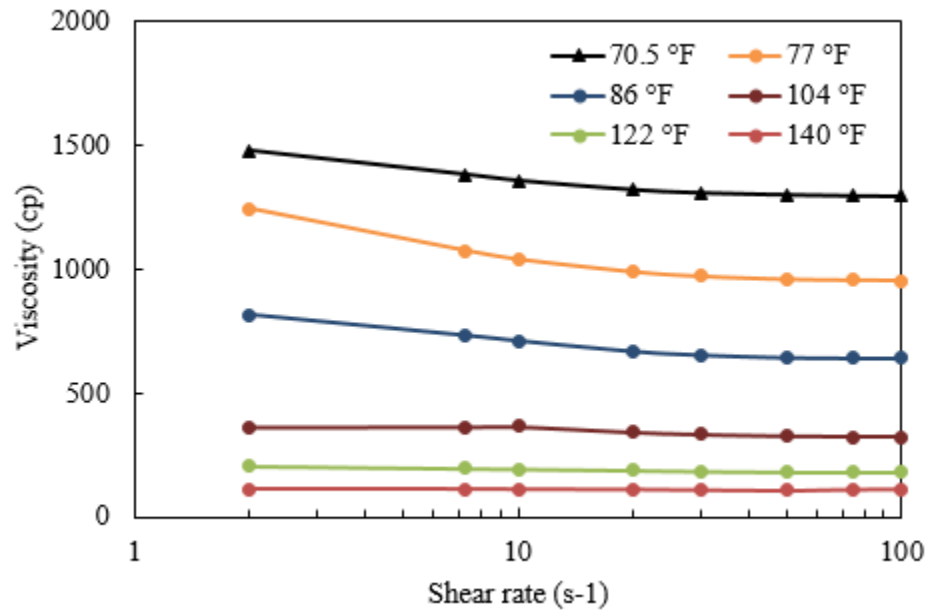
Figure 9 Viscosity of L-47 crude oil at different shear rates (70.5-140ºF).
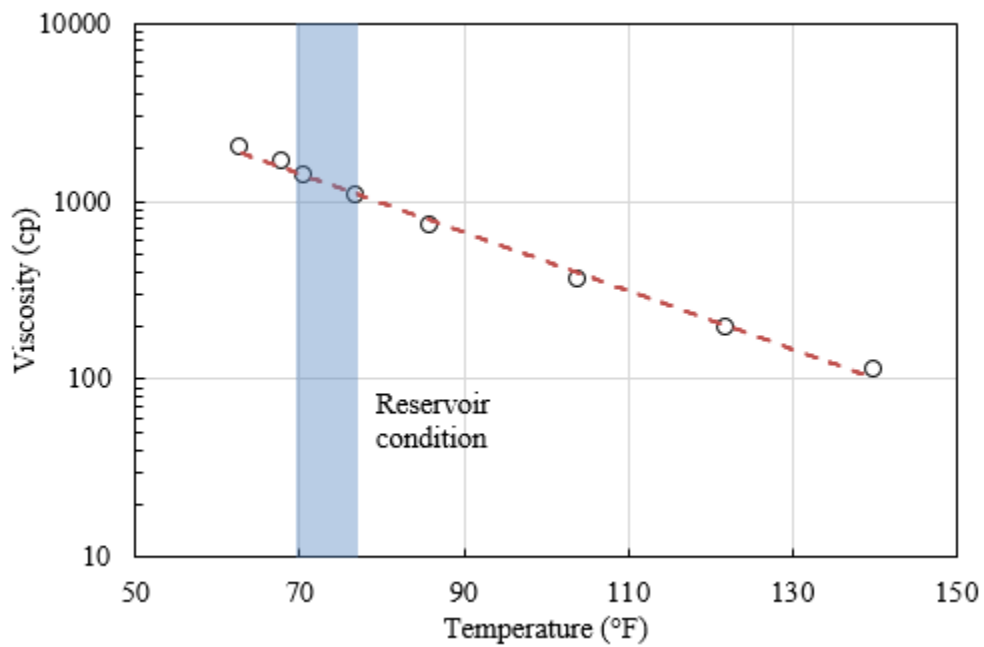
Figure 10 Viscosity of L-47 crude oil at different temperatures.

Polymer Viscosity

15

Two polymer solutions with different salinity were prepared and filtered through 1.2 µm filtration paper. The salinities were 26,673 ppm and 4,945 ppm respectively. The former was prepared with synthetic formation water, and the latter was prepared with synthetic injection brine (LowSal water). **Figure 11** shows the viscosities of the two polymer solutions. It can be seen that the LowSal polymer has higher viscosity than the one with conventional salinity. **Figure 11** also shows that both polymer solutions exhibit shear-thinning behavior.
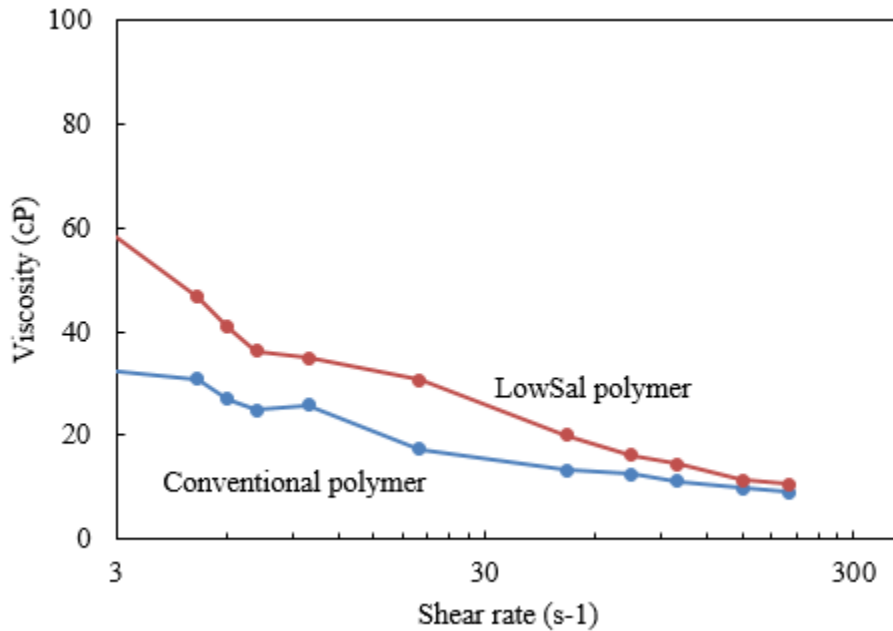
Figure 11 Viscosity of polymer solutions at different shear rates.

Effect of Salinity on Residual Oil Saturation through Sandpack Flooding Experiments
Sandpack experiments were carried out to study the effect of salinity on residual oil saturation. Commercial sand was used to prepare the sandpacks. The B-28 crude oil was used in the experiments. The parameters of the sandpacks and displacement fluids are summarized in **Table 2 and 3** respectively.

Table 2 Parameters of tested sandpacks.

Parameter	Sandpack A#	Sandpack B#
d, cm	2.54	2.54
L, cm	20.4	20.4
porosity	0.355	0.260
K, md	655	207

Table 3 Characteristics of displacement fluids used in the sandpack experiments.

Flood process	Displacing Fluid	Description	Salinity

16

			(ppm)
WF	Synthetic formation water	Synthetic formation brine (SFB)	26,673
LSWF	Low salinity water	Synthetic injection brine	4,945
ULSWF	Ultra-low salinity water	LSW diluted by 10 times	495
PF	Polymer solution	1800ppm FP3630S prepared with SFB	/
LSPF	Low salinity polymer (LSP)	1800ppm FP3630S prepared with LSW	/

Results and Analysis
Sandpack A# Experiment
The experimental procedure is summarized as below:
(1)   Dry the sandpack at 120°C for 48 hours and measure the dry weight.
(2)   Saturate the sandpack with synthetic formation brine. In this step, the sandpack was vacuumed first. Then the sandpack was saturated with brine by imbibition method. 5 PV brine was injected to further saturate the sandpack. The weight was measured. The pore volume was calculated with dry weight, wet weight and brine density.
(3)   Measure the absolute permeability with synthetic formation brine. Four injection rates, 0.5, 1, 1.5, 2 mL/min, were used to measure the absolute permeability. In each injection rate, stable pressure was reached. The absolute permeability was calculated using Darcy's equation. *Note that cc = cm^3 = mL, which has been variously used in the report*.
(4)   Saturate with crude oil (B-28). 5 PV crude oil was injected into the sandpack at 0.2 mL/min.
(5)   Age the sandpack for 4 days at 70ºF (reservoir temperature).
(6)   WF: 0.1 mL/min until water cut leveled at 100%.
(7)   LSWF: 0.1 mL/min until no was oil produced.
(8)   ULSWF: 0.1 mL/min until no oil was produced.
(9)   LSWF: 0.1 mL/min until no oil was produced.
(10) WF: 0.1 mL/min until no oil was produced.
(11) PF: 0.1 mL/min until no oil produced.

Figure 12 shows the oil saturation change during the flooding process. **Figure 13** gives the water cut and oil recovery factor. The results indicate that LowSal can reduce residual oil saturation and increase oil recovery. Further reducing the salinity of injected water can slightly reduce residual oil saturation and increase oil recovery beyond the LowSal. Experimental data from sandpack A# also suggests that increasing the salinity after LSWF/ULSWF cannot achieve additional oil recovery. Polymer flooding, though at normal salinity, can further reduce the residual oil saturation and recover more oil left behind by water flooding.
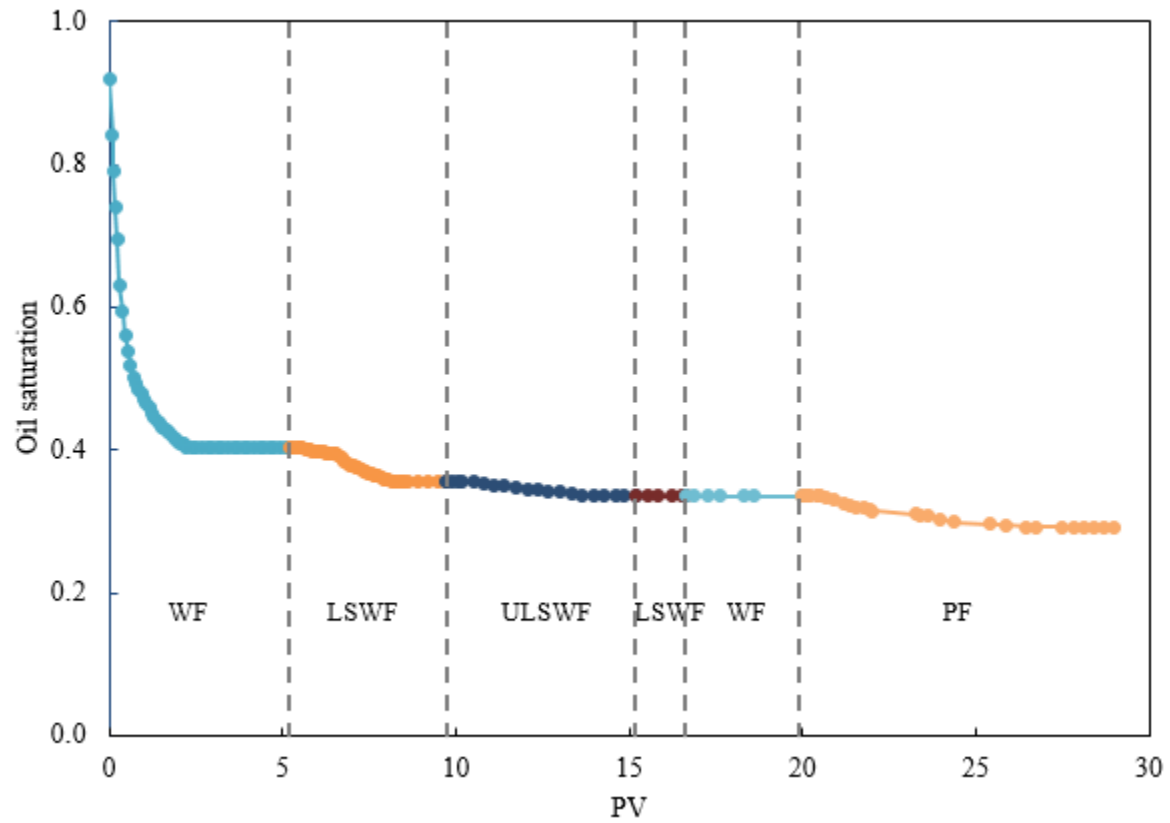
Figure 12 Effect of salinity on residual oil saturation (sandpack A#).

University of Alaska Fairbanks
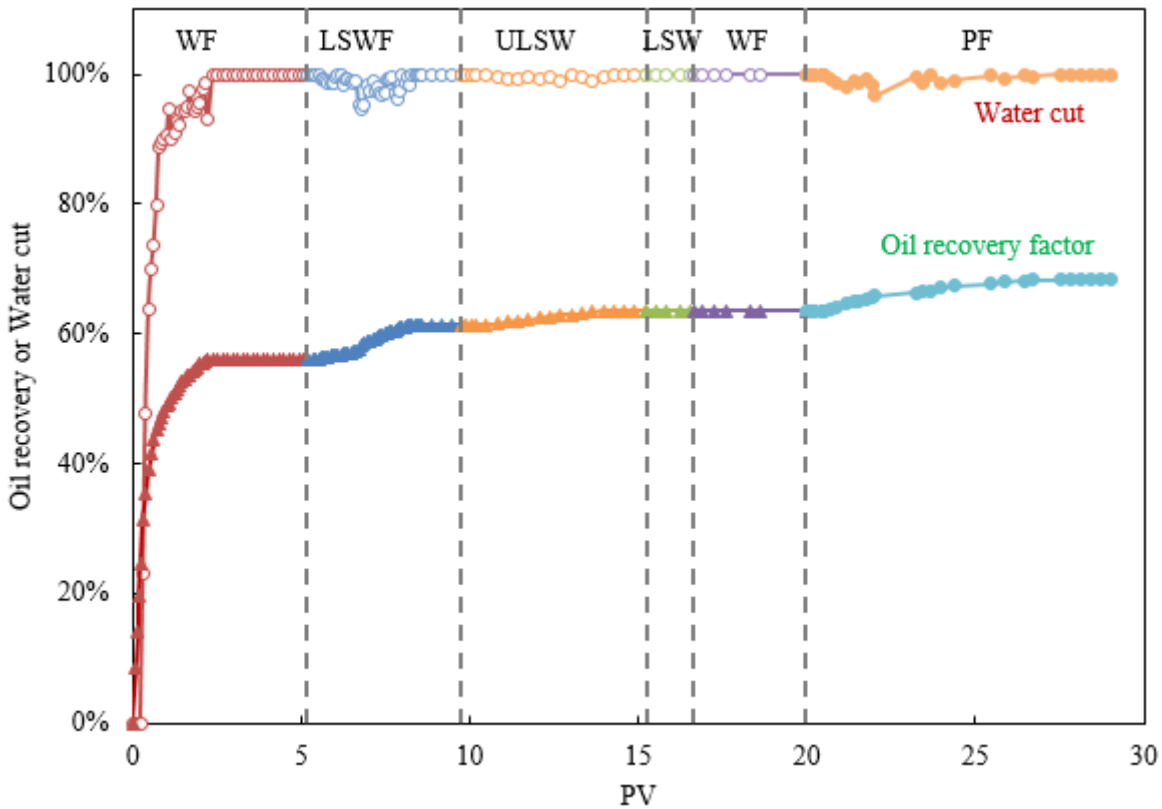
Figure 13 Water cut and oil recovery factor of sandpack A#.

Sandpack B# Experiment

The first five steps for these experiments are the same as sandpack A# but we injected different types of fluids to displace oil as shown in the following.

(1)   WF: 0.1-1 mL/min until water cut leveled at 100%.
(2)   LSWF: 0.1-1 mL/min until no was oil produced.
(3)   Softened LSWF: 0.1-1 mL/min until no oil produced.
(4)   LSPF: 0.1-1 mL/min until no oil produced.

Figure 14 shows the oil saturation change during the flooding process, and **Figure 15** shows the water cut and oil recovery factor. The results also indicate that LowSal can reduce residual oil saturation and increase oil recovery, which are consistent with sandpack A#. Interestingly, sandpack B# shows that oil recovery can also be slightly improved by reducing the hardness of injected LowSal water. Compared with sandpack A#, low salinity polymer flooding can achieve a better performance in reducing residual oil saturation compared with polymer flooding under conventional salinity condition.

19
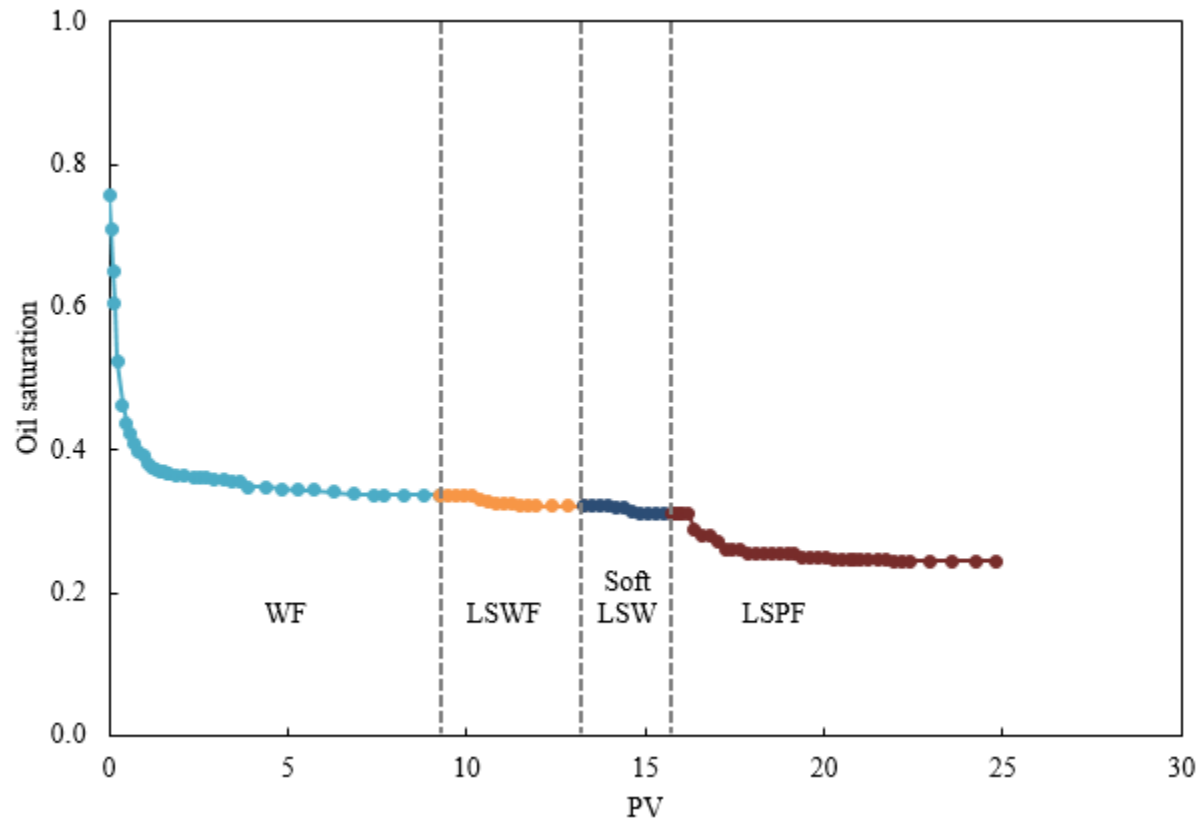
Figure 14 Effect of salinity on residual oil saturation (sandpack B#).
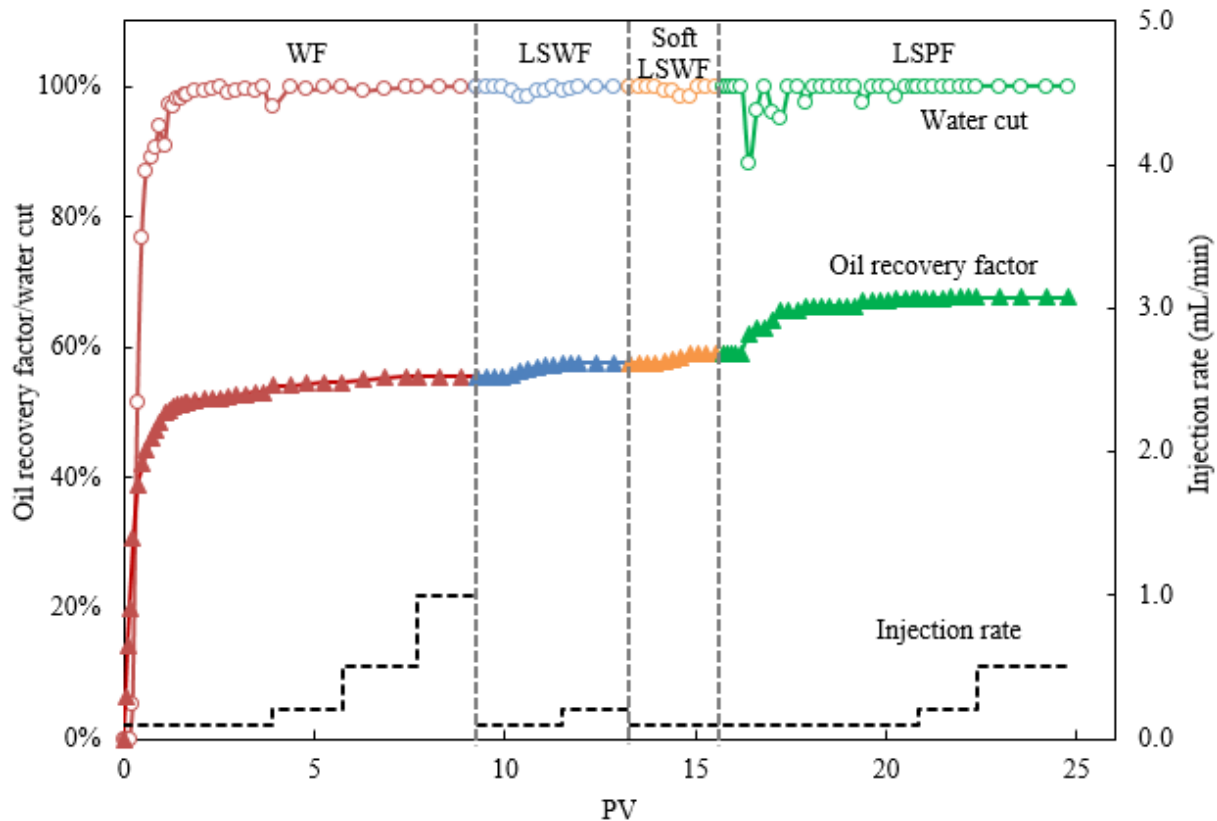
Figure 15 Water cut and oil recovery factor of sandpack B#.

Activity is ongoing.

● Task 4.0 - Reservoir Simulation Studies for Coreflooding Experiments and Optimization of Field Pilot Test Injection Strategy

Activities completed by UND during this quarter include:
- Polymer retention effects on polymer effectiveness simulations using 1-D model on laboratory sand pack experiment.
- Capillary pressure effects on polymer effectiveness simulations using 1-D model on laboratory sand pack experiment.

Simulation Model Establishment
In these cases, STARS of CMG (Computer Modeling Group) was selected as the numerical simulation model to build a $31 \times 1 \times 1 = 31$, 2 ft sandpack with an effective diameter of 1 cm, was characterized by 1-Dimension Cartesian grid blocks, with sealed boundaries and a laminar flow geometry allocation. The two wells were designated with an injection end and a production end as shown in **Figure 16**. There was no extended well spacing needed, due to numerical simulation principles and the actual laboratory sandpack flooding condition: a sealed reservoir boundary with no cross flow out of or into the

simulation area. Since the sand pack we were simulated was homogenous, 2-D or 3-D models were not need for this simulation. However, in the future, if the heterogeneity of sand pack or core plug will be used in the laboratory core flooding, 2-D and 3-D models will be built for the simulation purposes.

The initialization of numerical simulation was controlled by primary variables including phase saturation, phase mole fraction, and temperature and pressure. Phase appearance or disappearance causes variable switching that is determined by the numerical mathematical control method. Energy conservation was not imposed, and grid cell temperatures did not change from their specified initial values. Recurrent data, including polymer or water injection and production, was incorporated into the models, which were based on the experimental procedures.

Figure 16 1–D simulation model illustration for case studies.

Reservoir description

Grid block size was specified for the I, J, and K directions. The average sizes in the X- and Y-directions were 0.0645 ft. and 0.0328 ft., respectively, assuming the sand pack was homogenous in these cases. Each grid block had the same thickness in the Y- and Z-directions, since this case was designed as a 1-D model. The average well spacing between injector and producer (injection end from sandpack and producing end from sandpack) was 2 ft. Since the sand for these case studies was obtained from the NB formation, most of the reservoir parameters for simulation were determined according to the data sourced from this sand, but some parameters were revised based on the laboratory experiments when the simulation was focused on the experimental process. **Table 4** shows the reservoir parameters and the experimental data that were used in the case study for simulation.

Table 4 Reservoir parameters used for sandpack simulation.

Reservoir Parameter	Value*
Porosity, fraction	0.350
Permeability, md	1503
Rock compressibility, 1/psi	3.0E-6
Reference pressure, psi	14.7
Thermal conductivities	N/A

Reservoir pressure, psi	1,600
Reservoir temperature, °F	70
Surface temperature, °F	60

* Values were modified based on the actual experimental data

Fluid definition

Three components were considered in the polymer model: water, polymer, and heavy oil. Based on the simulation module (STARS) input requirement, the following parameters were described according to the actual reservoir and injection parameters: molecular mass, critical temperature, critical pressure, the liquid density and viscosity of each component, reservoir pressure and temperature, surface pressure and temperature (see **Table 5**). Among the keywords used in this section, 'VSMIXCOMP', 'VSMIXENDP' and 'VSMIXFONE' were used to specify non-linear mixes for the water phase when the polymer component was present. As a mobility control agent, polymer improves the mobility ratio by a combination of increased water phase viscosity and decreased effective permeability by blocking the pathways. The propagation characteristics are further affected by dispersion, adsorption and inaccessible pore volume. Polymer viscosity is non-Newtonian (shear rate dependent).

The original formation water salinity was 27,000 ppm, and the injection polymer solution salinity was 4,967 ppm. Reservoir temperature was 70°F. Polymer molecular weight was 18×10^6 Daltons based on the product used in the oil field. The initial polymer viscosity was 45 cp. The compositions of key components used nonlinear mixing of the water and polymer solutions to determine intermediate viscosities. A liquid viscosity of water, polymer and oil versus temperature, polymer rheology (shear thinning and shear thickening) was included.

Table 5 Fluid parameters used in the cases for simulation.

Component name	Water	Polymer	Heavy oil
Molecular weight, Mw, g/gmol	18	18×10^6	389.12*
Critical pressure, psi	3.20	3.20	377.70**
Critical temperature, °F	705.47	705.47	539.45**
Mass density, lb/ft^3	62.97	62.97	58.62

Compressibility, psi^{-1}	3.0E-5	3.0E-5	3.0E-5
Viscosity, cp	0.90	45.00/40.73 (lab)	140 (dead oil)

* Oil properties data sourced from the Well B-28. °API =19, Oil density =939.08 kg/m^3 = 58.62lb/ft^3

**The values for critical pressure and critical temperature estimation were established based on the "Liviano-01 sample 1.12- PVT report", the major hydrocarbons are "Hexanes$^+$, Heptanes$^+$, and Decanes$^+$.

Rock-Fluid properties

Prior to polymer flooding, the initial water saturation was assumed to be 0.20, the residual oil S$_{or}$ was 0.35; the critical gas saturation was set to 0.002. All of the above end point values for the relative permeability curves are adjusted according to the laboratory core flooding experimental data. Here, the relative permeability data were sourced from the NB sand at 4186.6 ft (water-oil table) and 4184.9 ft (gas-oil table). The curves are shown in the **Figure 17 and 18**.
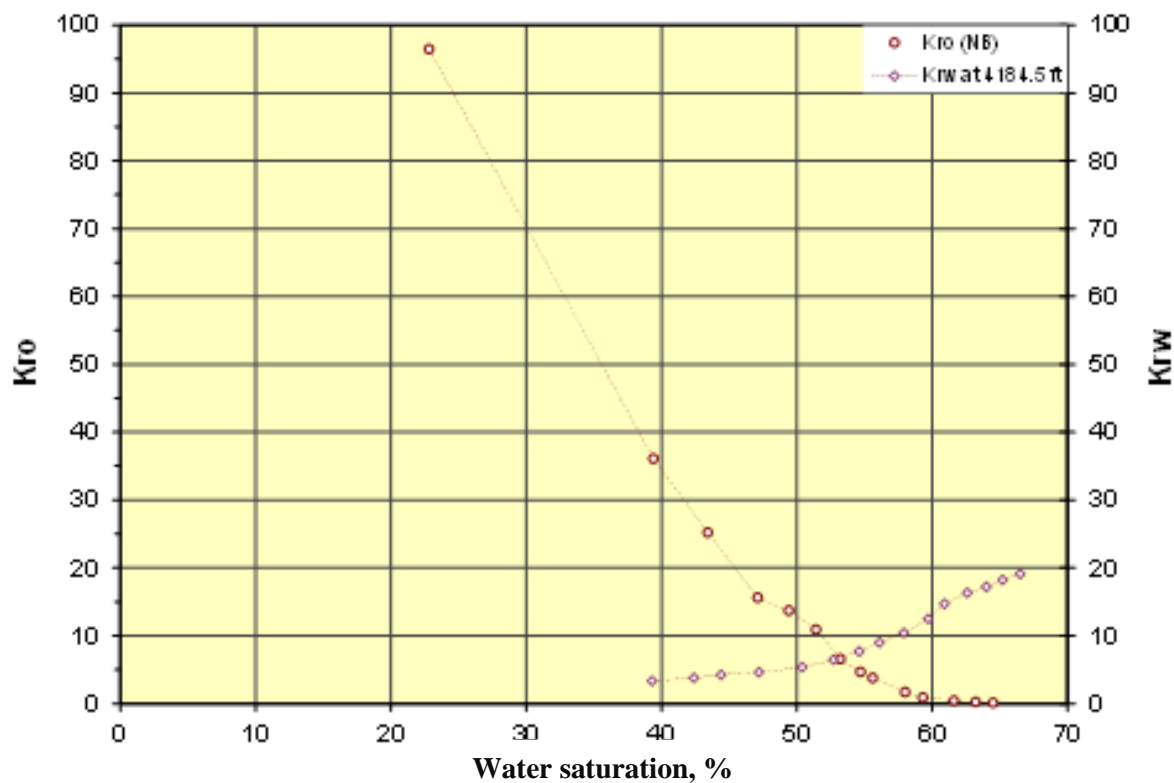
Figure 17 Oil-water relative permeability curves for case studies.
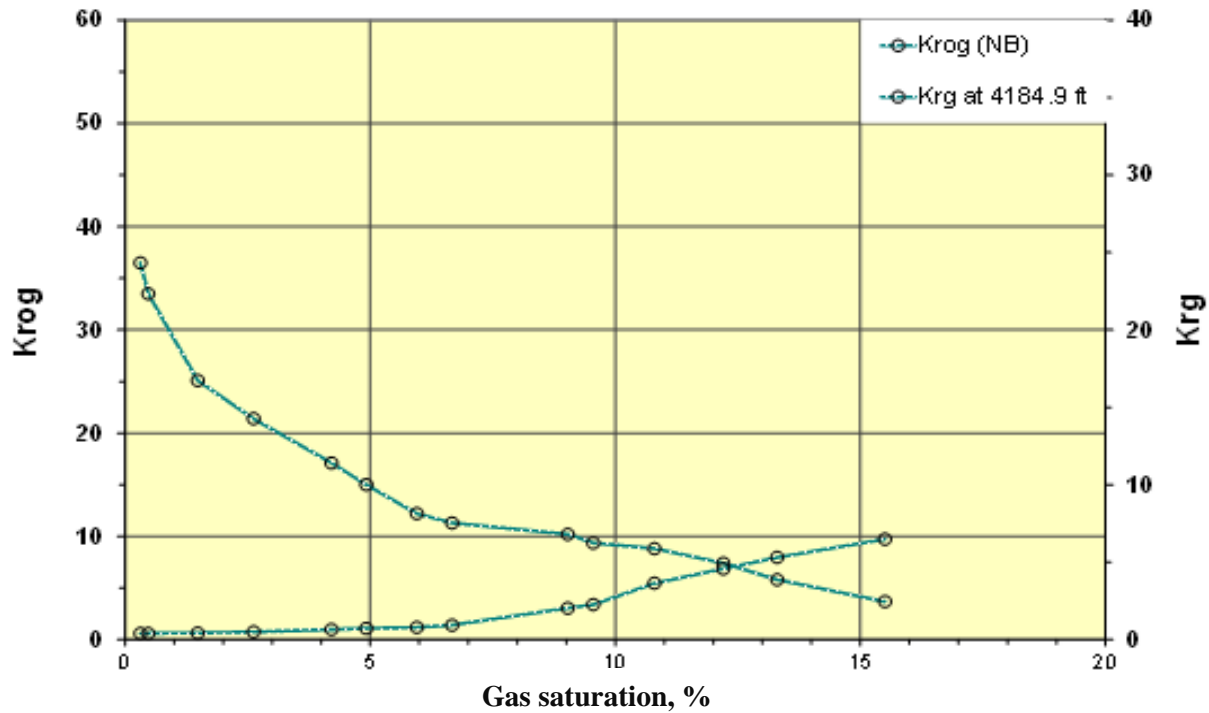
Figure 18 Gas-oil relative permeability curves for case studies.

Initialization
In the initial condition of the simulation model, only the initial mole fractions of the components in the water phase and heavy oil phase were considered, while mole fractions of the components in the gas phase were initially absent due to the laboratory experimental assumption (no gas). The formation pressures for experimental and field conditions were set to 14.7 psi, and 4,980 psi, respectively. For the first polymer retention measurement based on the lab conditions, initial settings for water and oil saturation were 80% and 20%, respectively; for the second measurement, the settings were 100% and 0%, respectively.

Numerical control
Phase saturations, phase mole fractions, and temperature and pressure were the primary variables. Phase appearance or disappearance caused variable switching by the numerical mathematical control method. Energy conservation was not imposed and grid cell temperatures did not change from their specified initial values. However, a keyword "SHIFT MWT" was employed in the numerical section. This keyword was used to scale shift values for the polymer component mole fractions and to help prevent numerical convergence difficulties due to the polymer adsorption capacity presenting a very small value when it was converted to a mole fraction.

Recurrent data
The recurrent times included a value of 24 mL/hr (29.7 ft/day) for the injection rate and a variable

injection pressure. In our simulation of the laboratory experimental procedures, the total injection slugs had reached 11 to 12 PVs when the polymer solution broke through the production end. All the injection pressures used in the models were simulated based on the experimental procedures.

Polymer Retention Simulation
Two cases of polymer retention were simulated for oil sand and clean sand based on laboratory experimental results. **Table 6** shows the parameters used in these two cases. All parameters are consistent with the laboratory experimental data.

Table 6 Parameters used for polymer retention simulation.

Reservoir Parameter	Values used in models	
	Oil sand, $S_{oi} = 0.20$	Clean sand, $S_{oi} = 0$
Porosity, fraction	0.409	0.370
Permeability, md	11,250	6,300
Pore pressure, psi	14.7	14.7
Polymer molecular weight–M_w, Dalton	18×10^6	18×10^6
Polymer concentration, ppm	1,750	1,750
Polymer viscosity, cP	40.73	40.73
Polymer retention, $\mu g/g$	290	153
Resistance factor, fraction	1	1
Inaccessible pore volume, ft^3	0	0
Initial water saturation, fraction	0.8	1.0

Adsorption parameter impact

Generally, there are two keyword options for polymer retention simulation using CMG modeling: the first is ADSLANG, in which the composition dependence is specified via the Langmuir isothermal coefficient. **Equation 1** describes how the adsorption capacity is calculated when polymer retention occurs in reservoir sands.

$$ad = [(tad1 + tad2 * xnacl) * ca]/(1 + tad3 * ca) \qquad (1)$$

where *tad1 – tad3* are the first, second and third parameters respectively in the Langmuir expression for the adsorption isotherm; *xnacl* is the formation water salinity and *ca* is the mole fraction of the polymer.

Because *tad1, tad2,* and *tad3* are obtained based on experimental parameters other than those of the targeted reservoir, errors may occur during simulations. Therefore, the second keyword option for polymer retention simulation (ADSTABLE) was used in the above cases. In ADSTABLE, the composition dependence is specified via a table of adsorption versus composition. In this option, the mole fraction of the polymer that is adsorbed is expressed in moles per unit pore volume which depends on the polymer concentration. In additional to the keyword selection on retention, residual adsorption capacity (ADRT) was set to the maximum capacity (ADMAXT) in the case studies. In other words, the polymer adsorption is completely irreversible.

Figure 19 and 20 are a comparison of the results using the two different keywords to describe polymer retention. As seen in **Figure 19**, using the ADSTABLE option, when the polymer broke through the production end, the polymer adsorption capacity was consistent with the experimental result of 3.8E-9 lbmole/ft^3, which corresponds to the mass value of 290 µg/g. However, when we kept all other conditions the same and used the ADSLANG option, a polymer adsorption value of 5.7E-10 was obtained by simulation. The results did not agree with the laboratory experimental data. The value of 5.7E-10 was less than the actual measured polymer retention by at least a magnitude of 10^{-1}. Furthermore, under the same injection pore volume, the polymer solution did not break through the production end as indicated in the colored scaling (**Figure 20**). In other words, polymer retention was effectively zero using the ADSLANG option — which we know was not correct for this case, based on the experimental data.
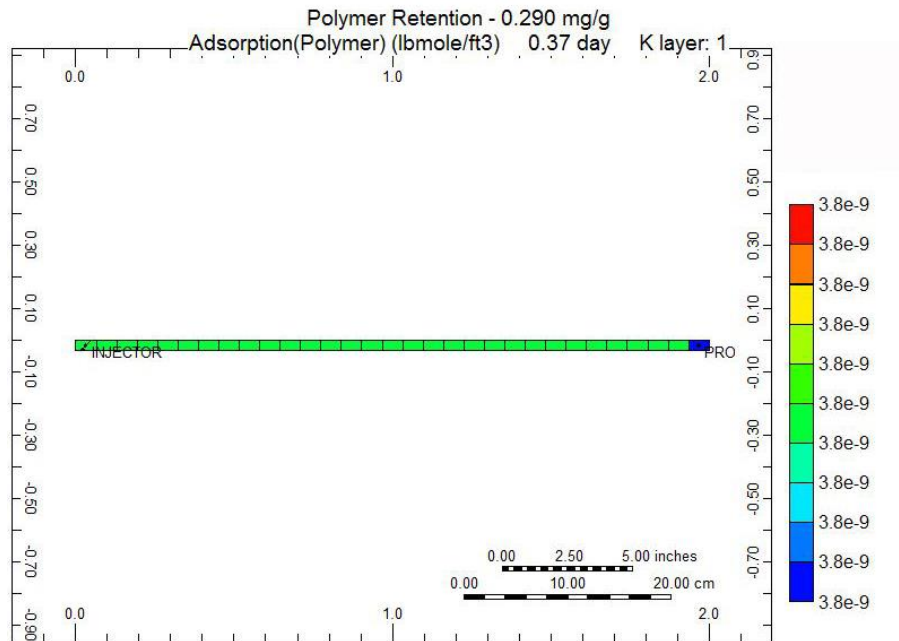
Figure 19 Polymer adsorption using Langmuir isothermal coefficient in oil sand.
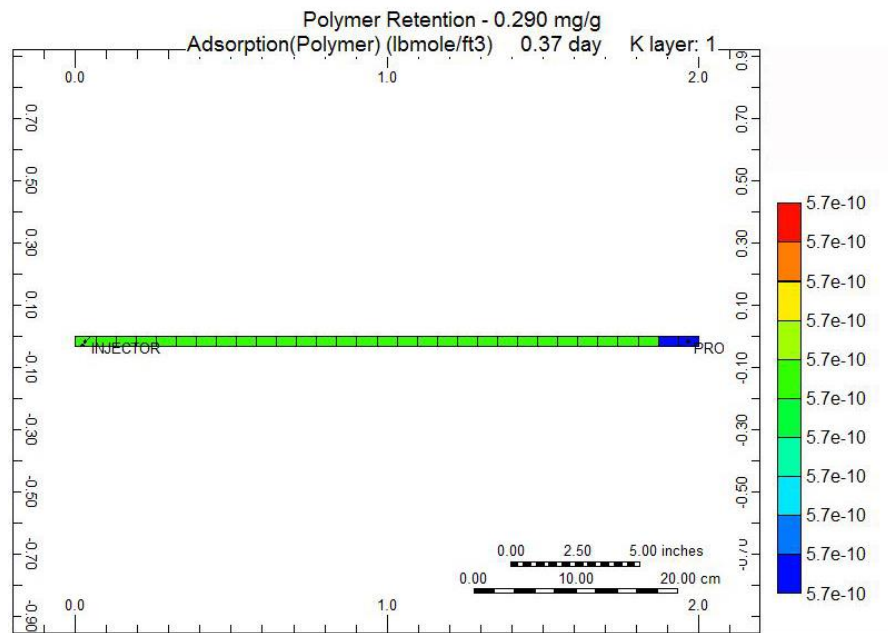
Figure 20 Polymer adsorption using the option of adsorption vs. composition in oil sand.
Adsorption capacity comparison
Figure 20 and 21 show the comparative polymer retention results in oil sand and clean sand using the option of adsorption versus composition. Based on the laboratory experimental results for oil sand (S_{oi} was 0.20), a retention of 290 µg/g for a 1750 ppm HPAM solution (Mw=18×10^6 gmol) delayed the

28

movement of the polymer front by 63%. In other words, for a polymer front to reach a given point in the core, the polymer bank that is injected into the reservoir must be 63% larger than without the retention. In this case, the retention resulted in an adsorption capacity of 3.8E-9 lbmole/ft^3 for the oil sand. For clean sand with a S_{oi} of 0.0, on the other hand, an adsorption of 153µg/g delayed the movement of the polymer front by 39%, and resulted in an adsorption capacity of 2.4E-9 lbmole/ft^3 (**Figure 21**). **Figure 22** shows a comparison of the solid volume change in the reservoir with the two retention values. As the figures show, adsorption caused by the solid volume change in the oil sand was about 1.78 times that of the clean sand when the polymer fronts reached the production end. This simulation result agreed with the range of delayed polymer slugs from 63% to 39%.
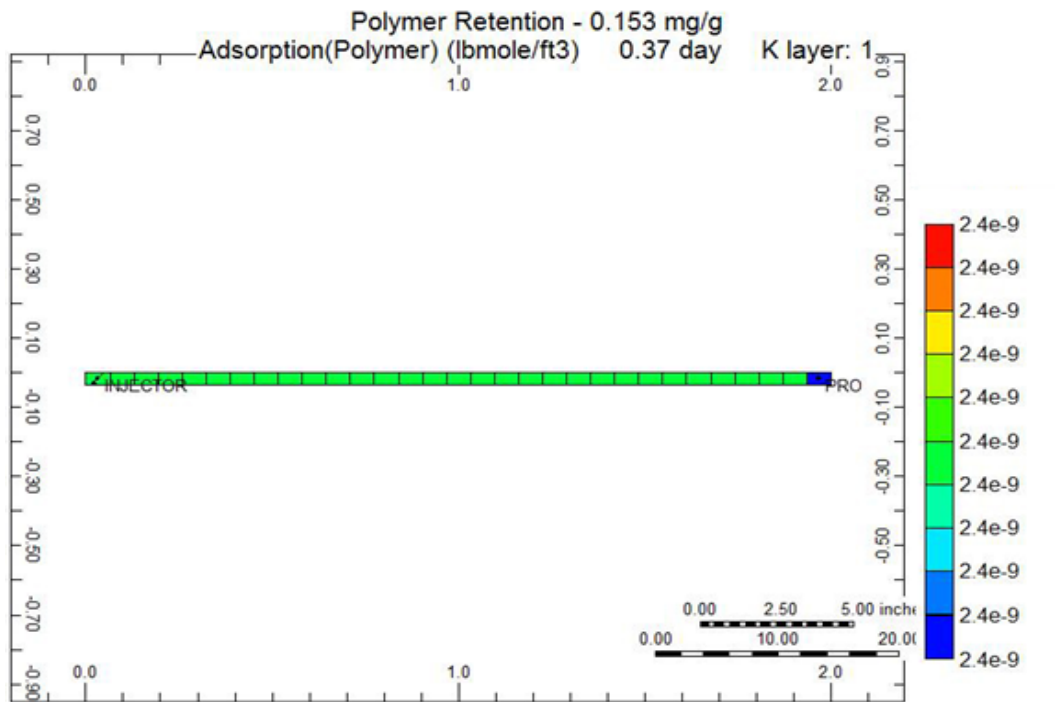
Figure 21 Polymer adsorption using the option of adsorption vs. composition in clean sand.
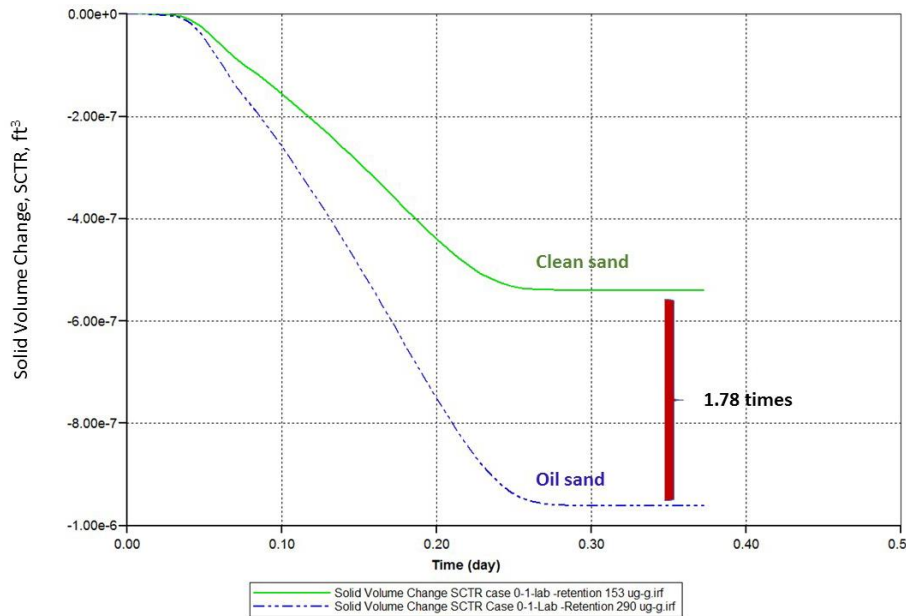
Figure 22 Comparison of solid volume change in oil sand and clean sand.

Capillary Pressure Impact

Capillary pressure effects on polymer retention were simulated using a polymer retention value of 290 µg/g in oil sand. A comparison was determined using the results from two simulation models: one model employed an extrapolated capillary pressure curve using the power regression mathematical method based on laboratory measurements of one core sample from the reservoir; the second model employed a default capillary pressure input - zero capillary pressure values. Based on the simulation results, the following observations were made: for the target heavy oil reservoir with high permeable oil zones and large pore size sand, there were no significant effects on polymer retention or fluid saturation using the 1-D sand pack model as shown in **Figure 23-25**.
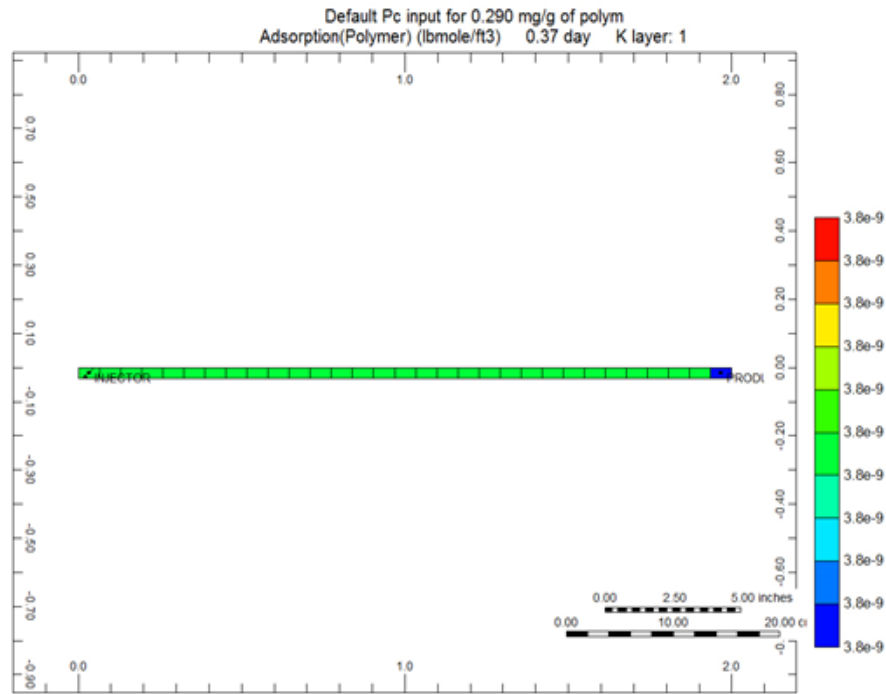
Figure 23 Polymer adsorption without capillary pressure input.
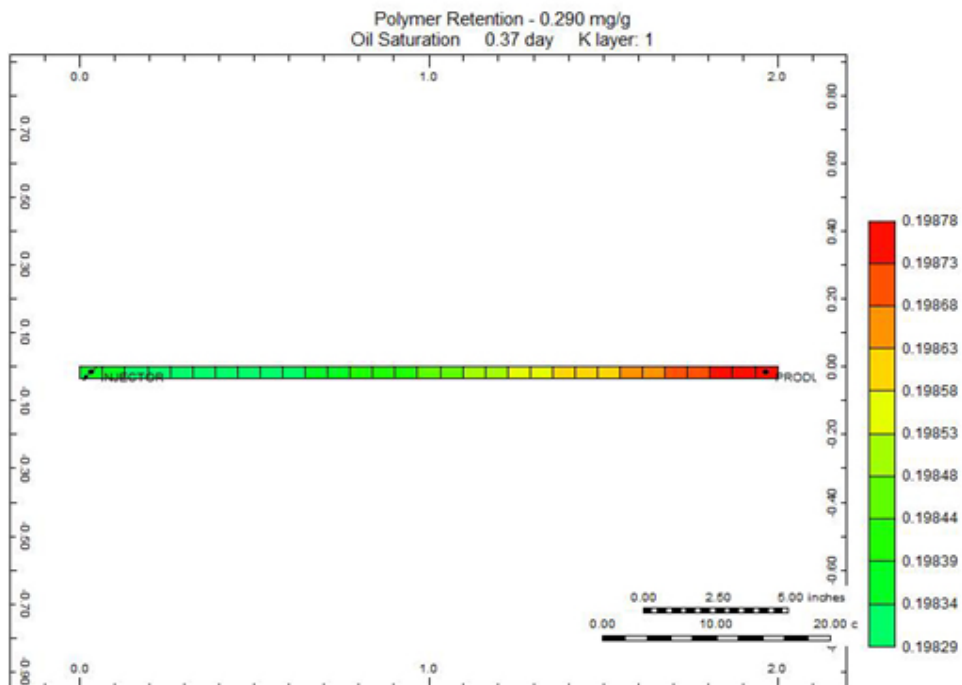
Figure 24 Oil saturation changes using the Pc-curve extrapolation method through a core test from reservoir.
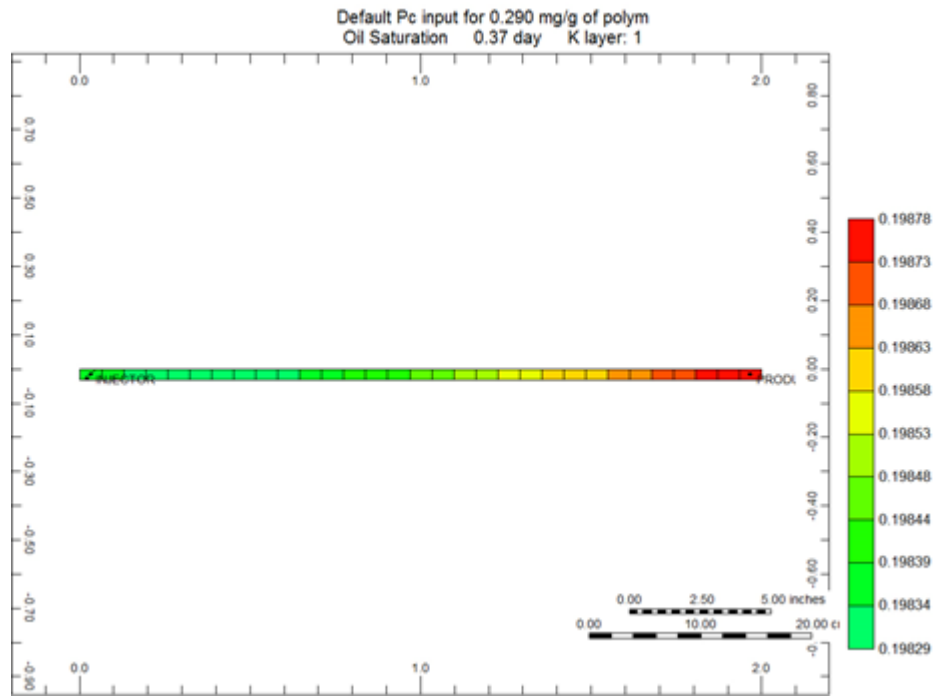
Figure 25 Oil saturation changes without capillary pressure input.

UND activity is ongoing.

UAF Work on field scale simulation

Initial reservoir simulation model
The 3D grid system of the initial reservoir simulation model has been generated based on the geological model provided by Hilcorp geologist. The following fluid properties, rock-fluid interaction data, and production data have been collected from Hilcorp Alaska.
- k_x/k_y and k_x/k_z
- reference reservoir pressure for fluid properties
- water properties: compressibility, viscosity, formation volume factor, salinity
- oil properties
- oil-water, oil-gas relative permeability and capillary pressure curves
- rock compressibility
- initial reservoir pressure and initial oil and water saturation
- well perforations data
- radii for injectors and producers
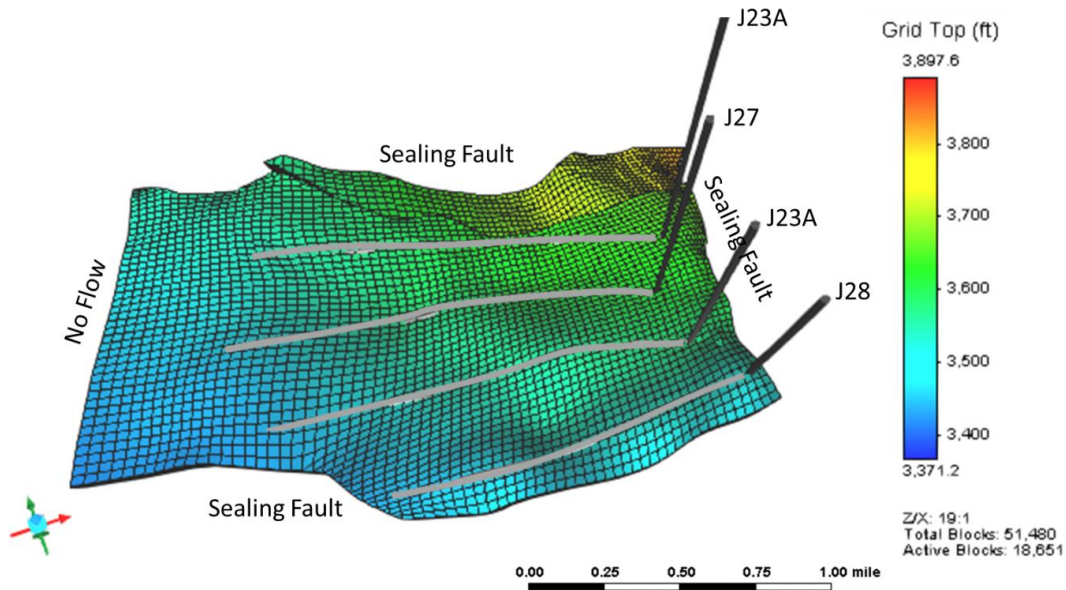
Figure 26 The grid top diagram of the initial reservoir simulation model.

By integrating the aforementioned data, the initial reservoir simulation model is established as shown in **Figure 26**. Since the water injection rate and the oil production rate are used as well constraints in the reservoir simulation model, only the water cut and gas production rate of two production wells need to be matched in the history matching process.

History matching of waterflooding
CMOST, a module of the CMG simulator, is used to conduct the history matching with the assistance of advanced algorithms. The permeability and the relative permeability curves are modified step by step to match the waterflooding production history. First, the homogeneous permeability in each layer is tuned in a layer cake model. Second, the relative permeability curves are tuned in a heterogeneous model. Finally, the permeability distribution in a strip manner is tuned with the estimated relative permeability curves.

Layer cake model
The layer cake model is shown in **Figure 27**. The permeability in each layer is homogeneous and initially assigned with the corresponding average permeability. In addition, the porosity of each layer is fixed at its average value. In the history matching, only the homogeneous permeability in each layer is varying from 100 mD to 7600 mD, which is in line with the core data. **Figure 28** shows that the oil production rates, i.e., well constraints, in the simulation models correspond to the actual ones. The history matching results are shown in **Figure 29**. The dots are actual field data and the black line represents the initial production response in the simulation model prior to the history matching. The red line is the production response of the best-matched simulation model.
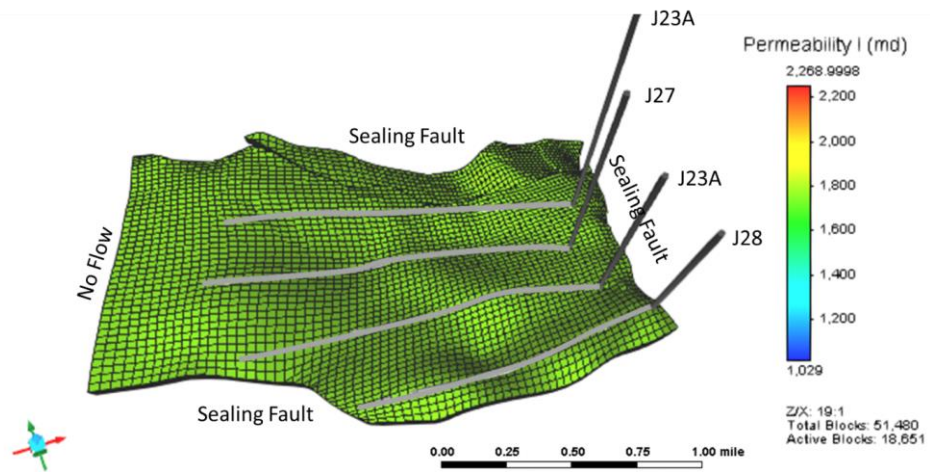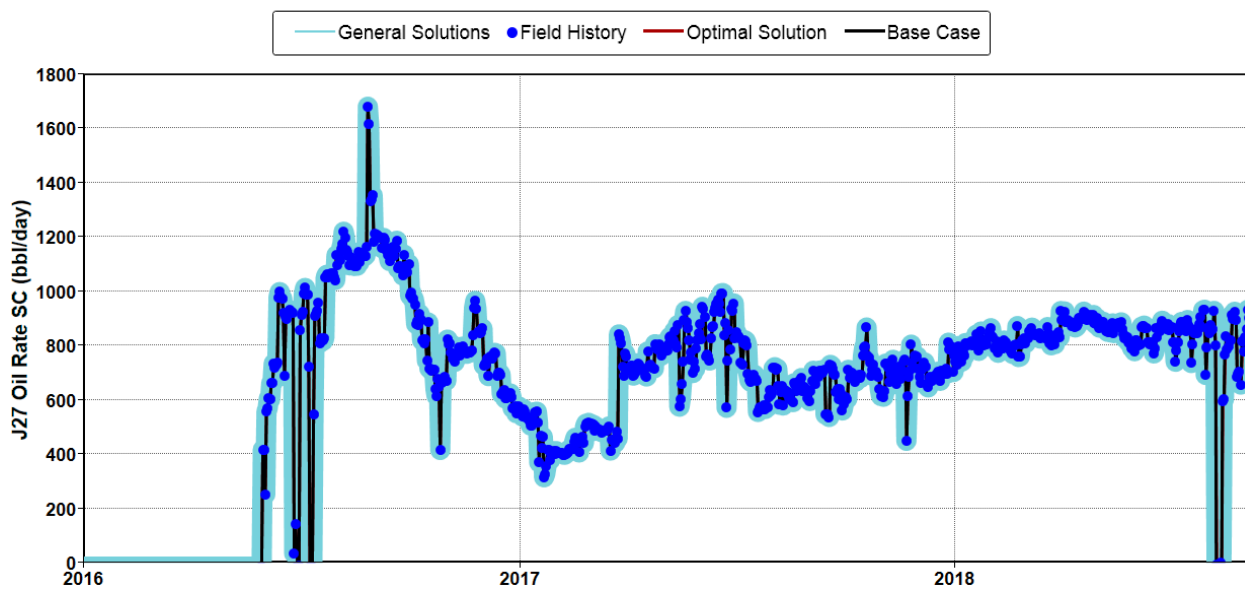
Figure 27 Layer cake model demonstrated by permeability distribution.

(a)

(b)
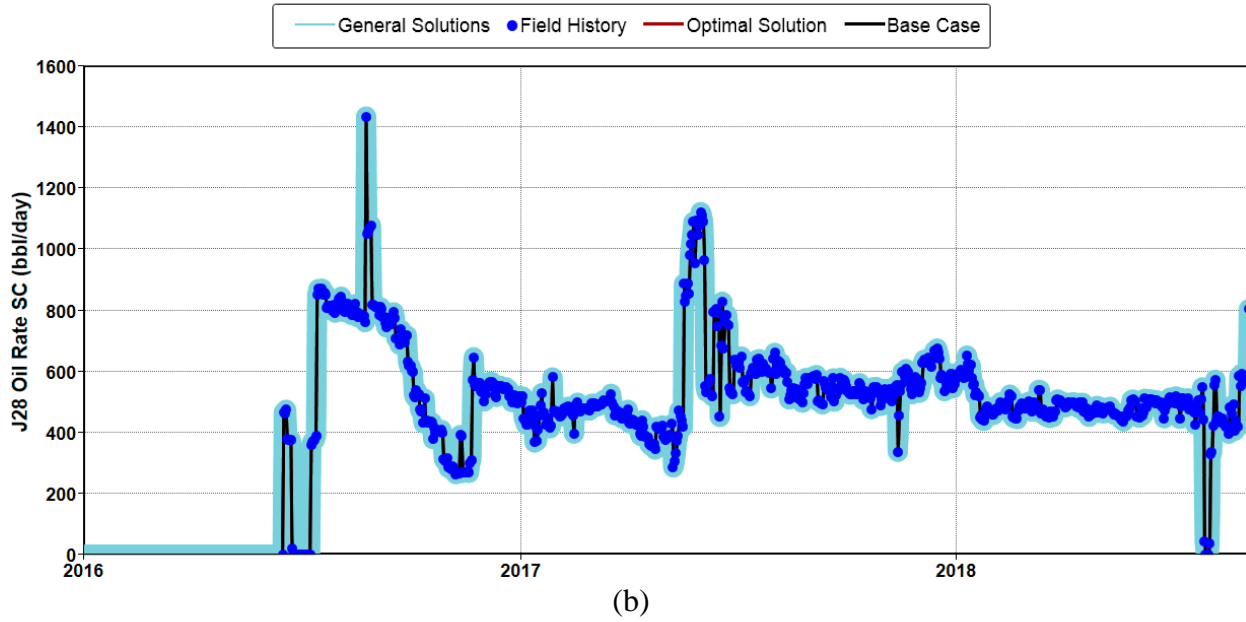
Figure 28 Oil production rates of J27 (a) and J28 (b) in the simulation models.

(a)

35

(b)

(c)

(d)
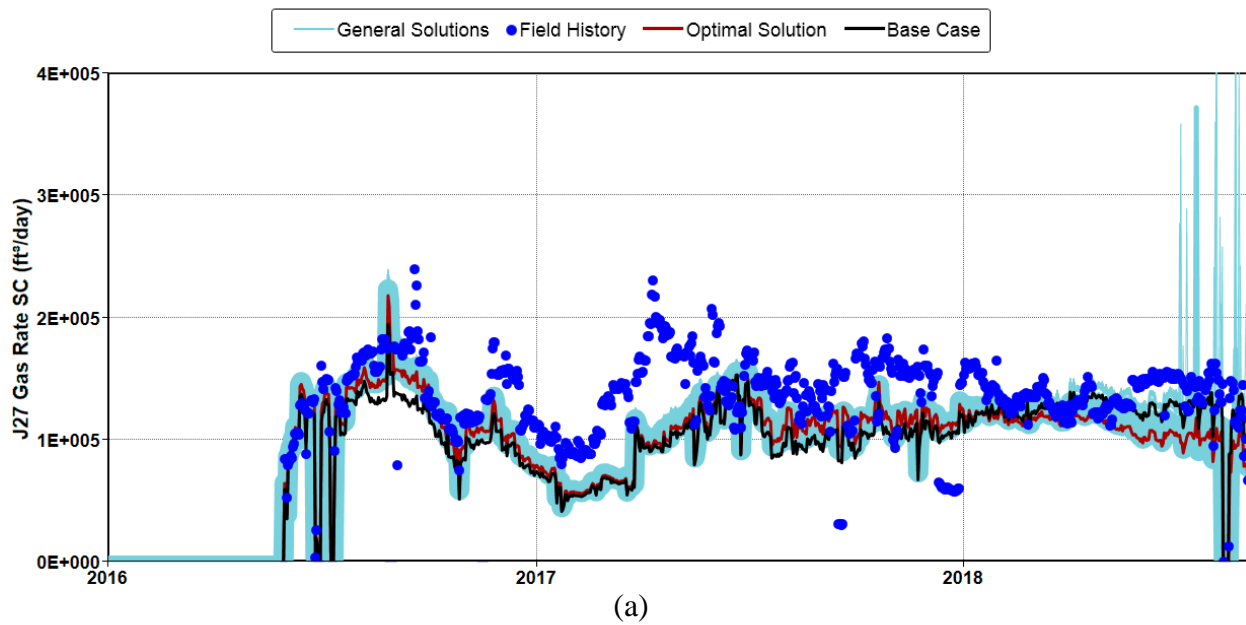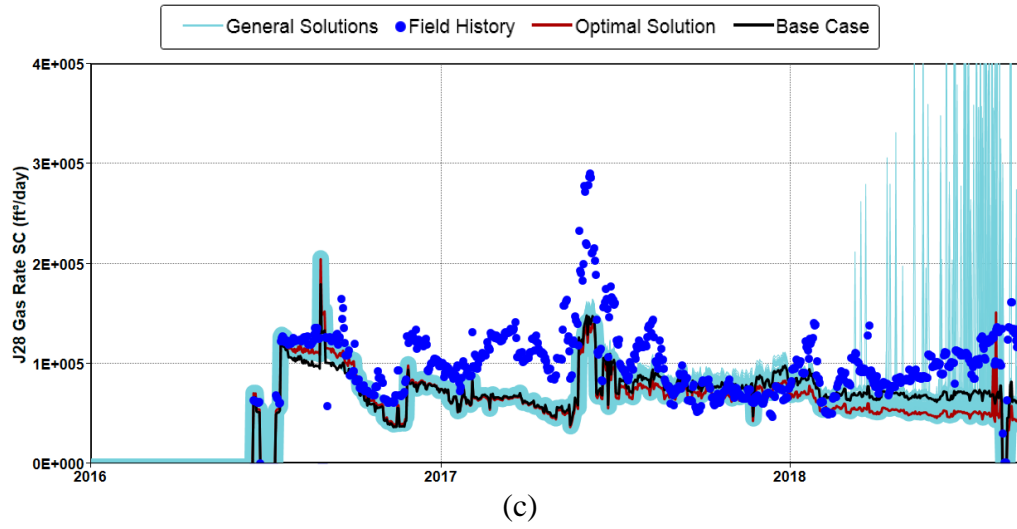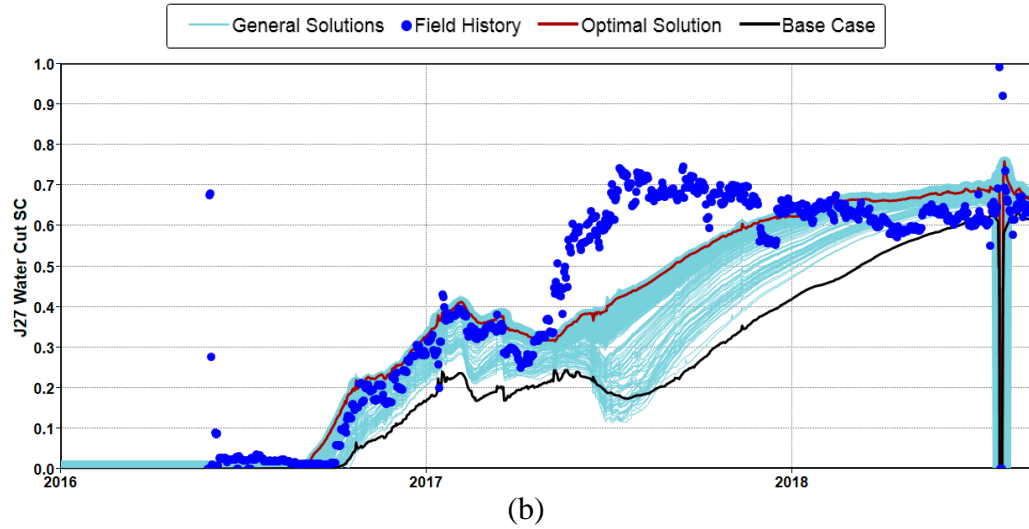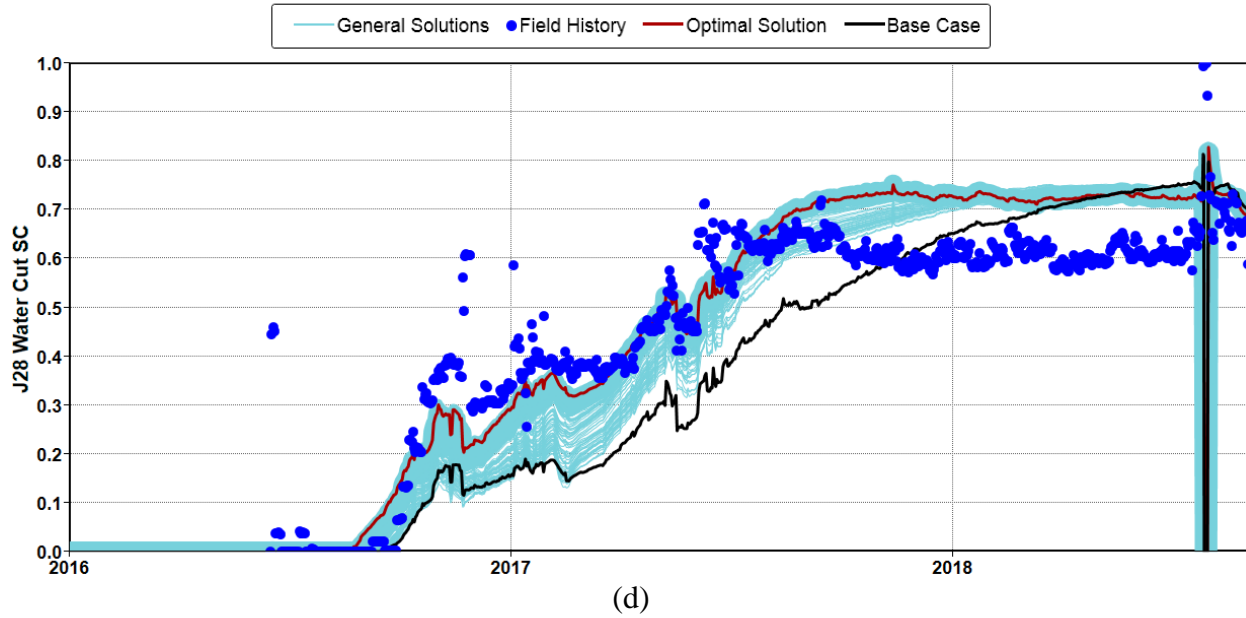
Figure 29 History matching results of (a) gas production rate and (b) water cut of J27 well and (c) gas production rate and (d) water cut of J28 well.

It has been found that using homogeneous permeability in each layer cannot reproduce the water cut curves with humps. To improve the history matching results, the permeability and porosity arrays provided by the geological model are used in the heterogeneous model.

Heterogeneous model
In this case, the relative permeability curves are tuned to match the water flooding production history. First, the relative permeability is parameterized by using the power-law model. For the oil-water system, the relative permeability is represented by:

$$k_{rw}\left(S_w\right)=a_w\left(\frac{S_w-S_{wi}}{1-S_{wi}-S_{orw}}\right)^{n_w} \tag{2}$$

$$k_{row}\left(S_w\right)=a_o\left(\frac{1-S_w-S_{orw}}{1-S_{wi}-S_{orw}}\right)^{n_{ow}} \tag{3}$$

where k_{rw} (S_w) and k_{row} (S_w) are the water- and oil-phase relative permeability, respectively; a_w and a_o are the maximum of water- and oil-phase relative permeability, respectively; S_w is water saturation; S_{wi} is irreducible water saturation; S_{orw} denotes residual oil saturation (to water); n_w and n_{ow} are the (Corey) exponents controlling the curvatures of relative permeability curves. As for the oil-gas system, the relative permeability is similarly expressed by:

37

$$k_{rg}\left(S_g\right) = a_g\left(\frac{S_g - S_{gc}}{1 - S_{wi} - S_{gc} - S_{org}}\right)^{n_g} \tag{4}$$

$$k_{rog}\left(S_g\right) = a_o\left(\frac{1 - S_{wi} - S_g - S_{org}}{1 - S_{wi} - S_{gc} - S_{org}}\right)^{n_{og}} \tag{5}$$

where $k_{rg}(S_g)$ and $k_{rog}(S_g)$ are the gas and oil-phase relative permeability, respectively; a_g is the maximum of gas-phase relative permeability; S_g is gas saturation; S_{gc} is critical gas saturation; S_{org} denotes residual oil saturation (to gas); n_g and n_{og} are the (Corey) exponents controlling the curvatures of relative permeability curves.

Based on laboratory measured core data, a_o and S_{wi} are set as 1.0 and 0.235, respectively. The other coefficients of the power-law model are directly tuned in the history matching process. The adjustment and estimate of these coefficients are shown in **Table 7**. It is worth noting that the realistic oil production rates are well reproduced in the simulation model. **Figure 30** shows the updated history matching results by optimizing the coefficients of the power-law model. A close agreement can be found between the simulated and the actual water cut curves for both J27 and J28 wells. In other words, the estimated relative permeability curves are able to capture the multiphase flow performance in the water flooding process to a large extent.

Table 7 Coefficients of power law model in history matching.

Variable	Base	Range	Best Estimate
S_{orw}	0.32	0.30-0.35	0.31
a_w	0.35	0.15-0.50	0.33
n_w	2.00	1.00-4.00	1.50
n_{ow}	2.00	1.50-4.00	2.70
S_{org}	0.20	0.10-0.30	0.20
S_{gc}	0.02	0.01-0.06	0.02
a_g	0.30	0.10-1.00	1.00
n_{og}	2.00	1.50-3.50	1.69
n_g	2.00	1.50-4.50	2.10

(a)

(b)
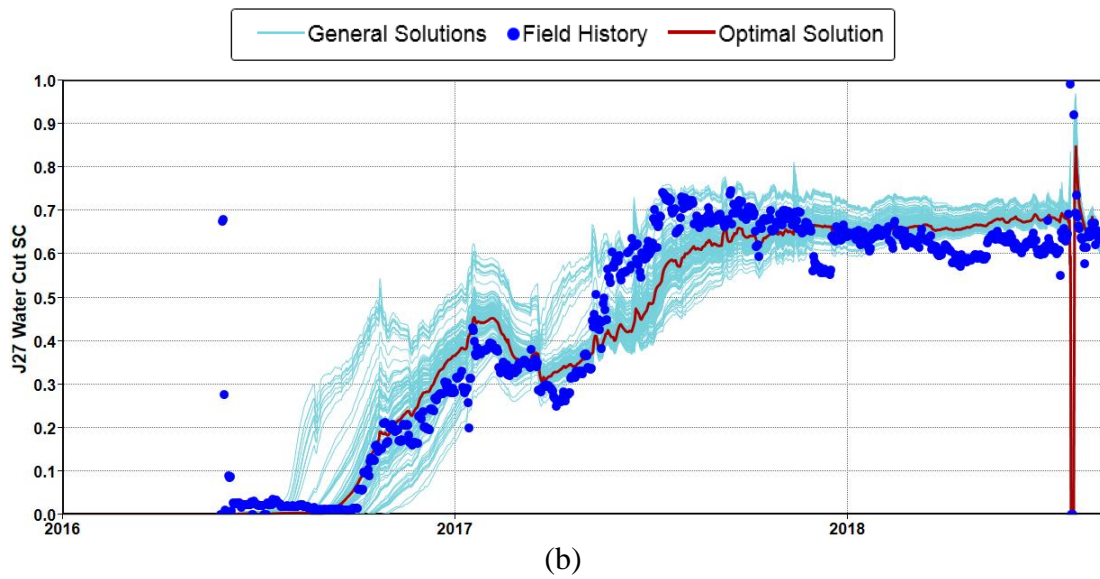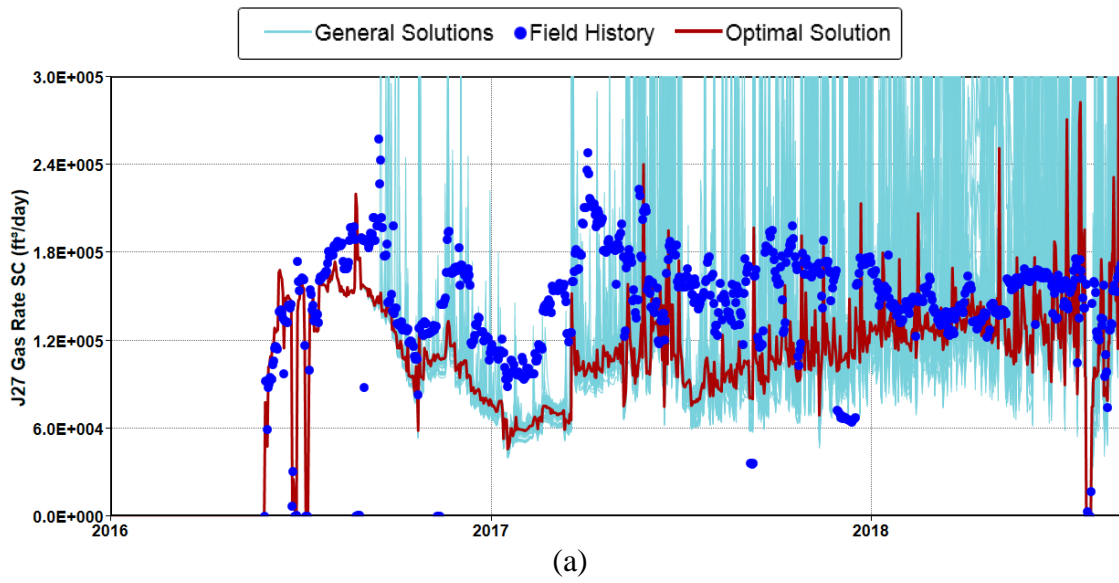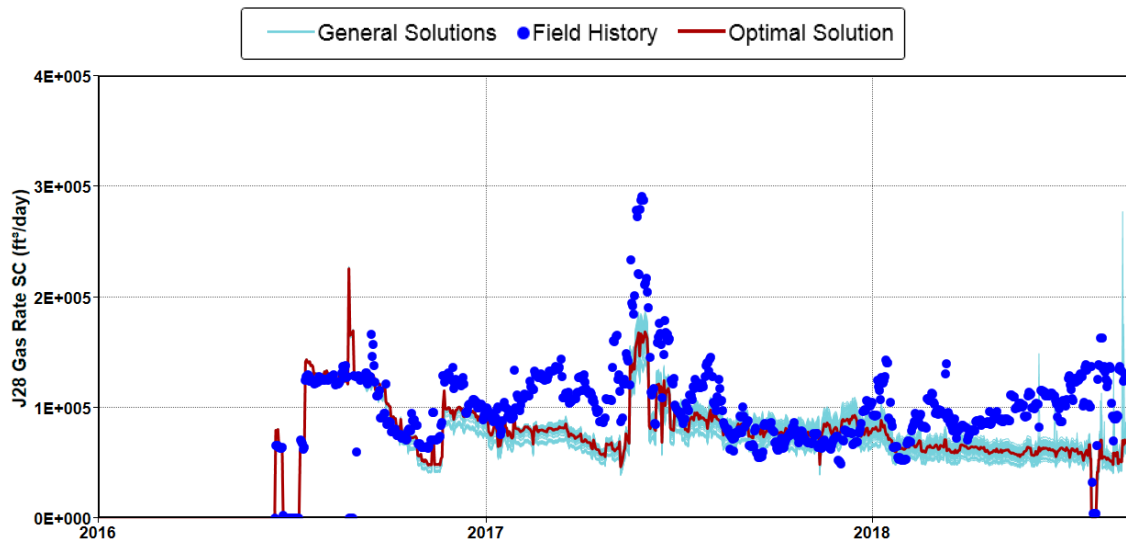
(c)
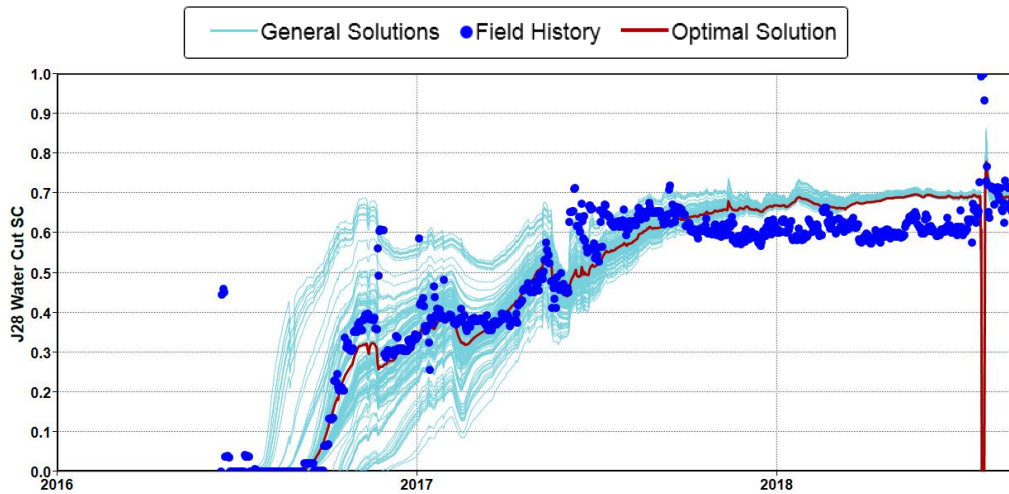
(d)

Figure 30 History matching of the production profiles of J27 and J28 by tuning the water-oil and oil-gas relative permeability.

Given the estimated coefficients of the power-law model, we have plotted the estimation of water-oil and oil-gas relative permeability in **Figure 31**.
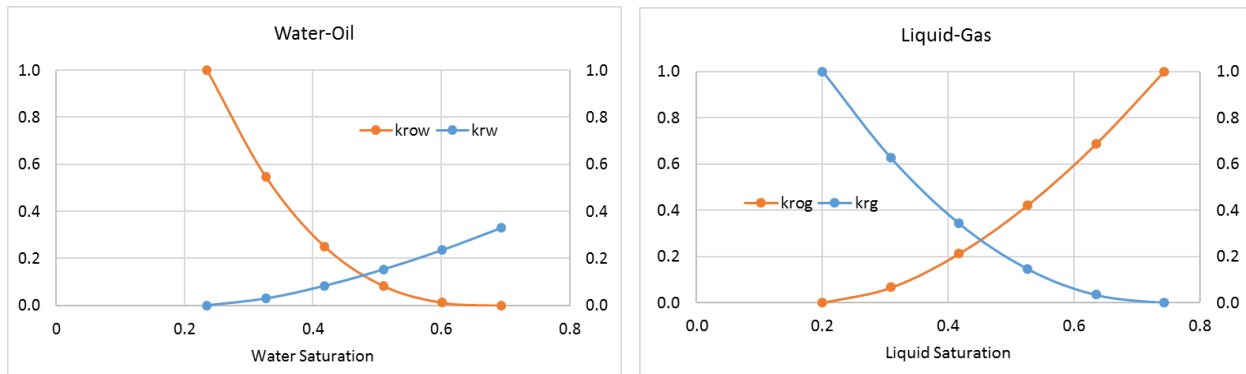
Figure 31 The estimation of water-oil and gas-oil relative permeability.

Permeability strip model

A permeability strip model is developed as shown in **Figure 32** to further investigate the heterogeneity of the field pilot reservoir. Nine permeability strips are assigned in each layer, resulting in 45 permeability strips in the simulation model. The permeabilities of the strips in each layer are initially assigned with the average permeability of the layer and then tuned between 100 and 7600 mD during the history matching process. In addition, the average porosity of each layer is used and the estimated relative permeability curves shown in **Figure 31** are also used in the simulation model.
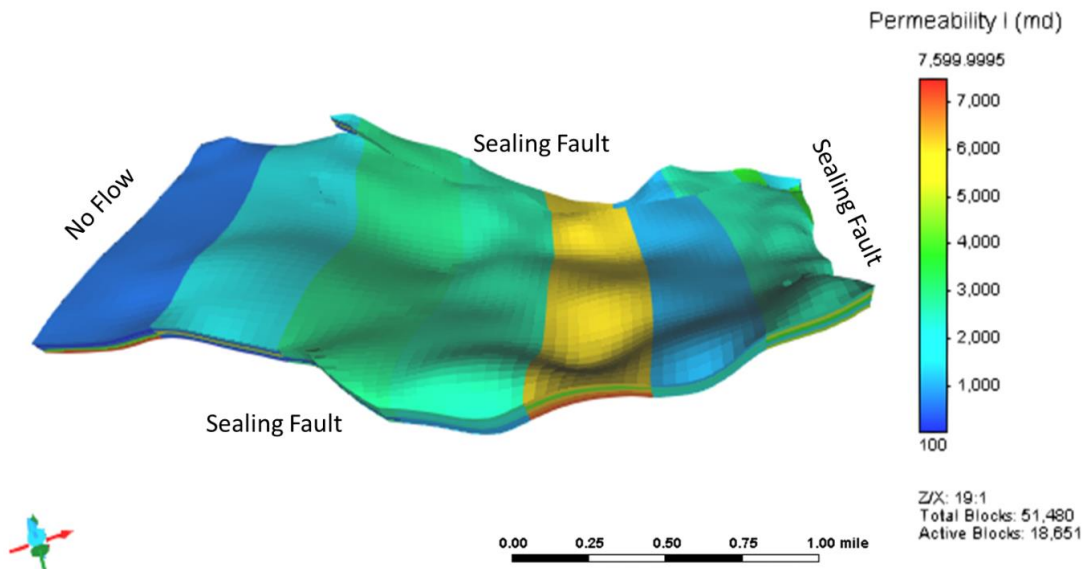
Figure 32 Permeability strips in the simulation model.

The actual oil production rates are also reproduced in the simulation model. The best history matching result in the permeability strip models are shown in **Figure 33**. The humps on the water cut curves have been well reproduced in the simulation due to the heterogeneous and strip-type permeability distribution.

41

Therefore, the estimated permeability strip model is to be used for the subsequent waterflooding and polymer flooding prediction.

(a)

(b)

(c)

(d)

42
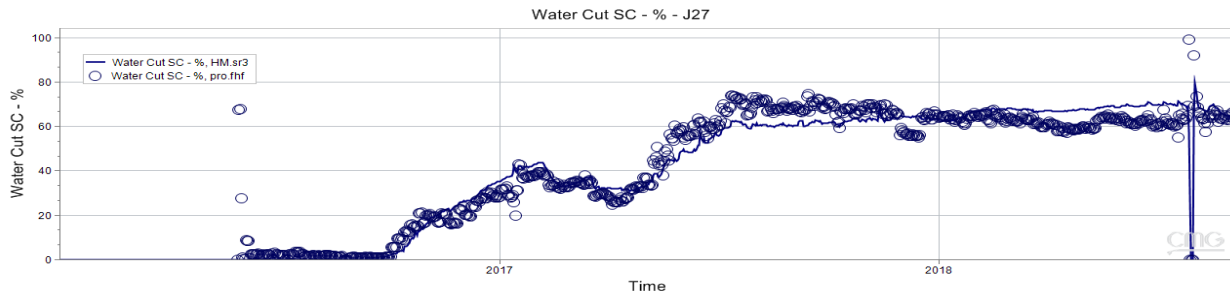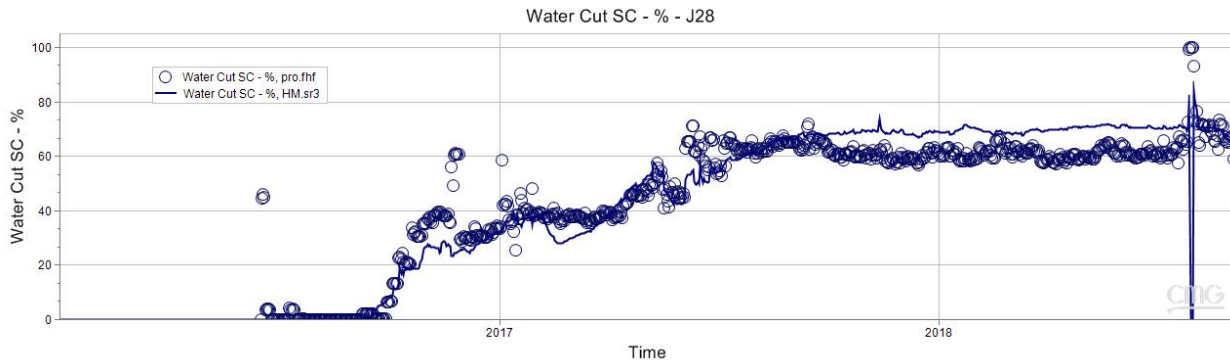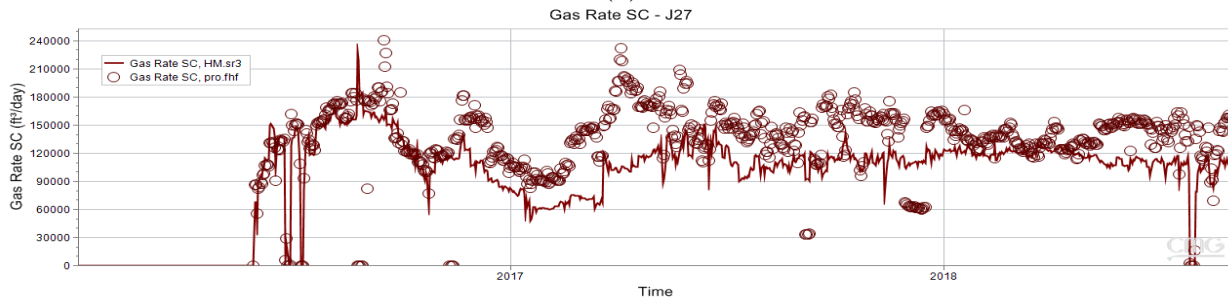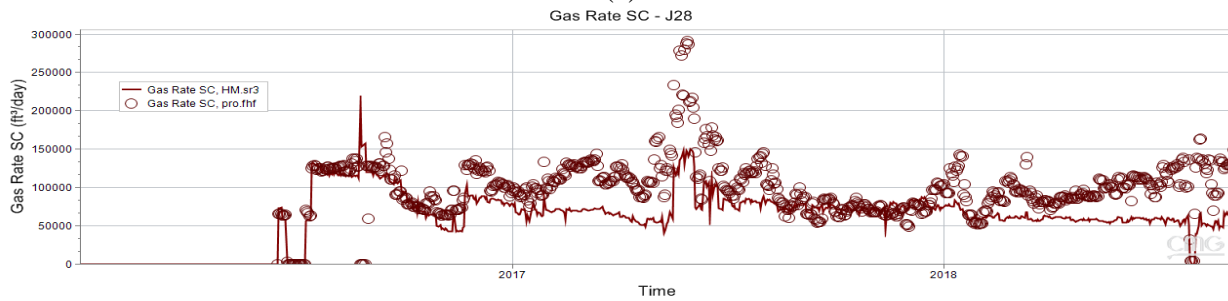
Figure 33 History matching of the production profiles of J27 and J28 in the permeability strip model.

Future work will focus on the following
1. Using the permeability strip model (shown in **Figure 32**) associated with estimated relative permeability curves (shown in **Figure 31**) to predict waterflooding and proposed polymer flooding performance;
2. Continue to update the reservoir model once the production data from polymer flooding becomes available.

UAF activity is ongoing.

● Task 5.0 - Implementation of Polymer Flood Field Pilot in Milne Point

Accomplishments
● Modified polymer skid to Class I Division II to accommodate gas released from source water;
● Performed post-polymer step rate test;
● Performed post-polymer pressure falloff test;
● Continued produced fluid sampling and analysis.

Polymer Injection Status Timeline
8/23 Polymer skid (PSU) online with water.
8/28 Polymer injection starts. Ramp up from 600 ppm (4 cp) to 1800 ppm (~45 cp).
9/7 Pump P-6000 failed, switched to spare pump P-8000 for J-23A.
9/25 PSU shutdown because more hydrocarbon gas found in source water than expected. Need to modify and reclassify PSU to Class I Division II to accommodate gas released from source water.
10/15 Resume polymer injection. Ran downhole gauge. Performed post polymer step rate test.
11/3 Pump P-8000 failed, J-23A took 1000 bpd without pump.
11/9 J-23A shut in for PFO while waiting for pump repair.
11/16 J-24A shut in for PFO while repairing augur.
12/3 Resume polymer injection into both injectors.

Polymer Injection Performance
As of November 30, 2018, cumulative polymer injected was 58,700 lbs into J-23A and 38,100 lbs into J-24A. Polymer concentration was between 1600 to 1800 ppm to achieve a target viscosity of 45 cp as

University of Alaska Fairbanks

shown in **Figure 34**.
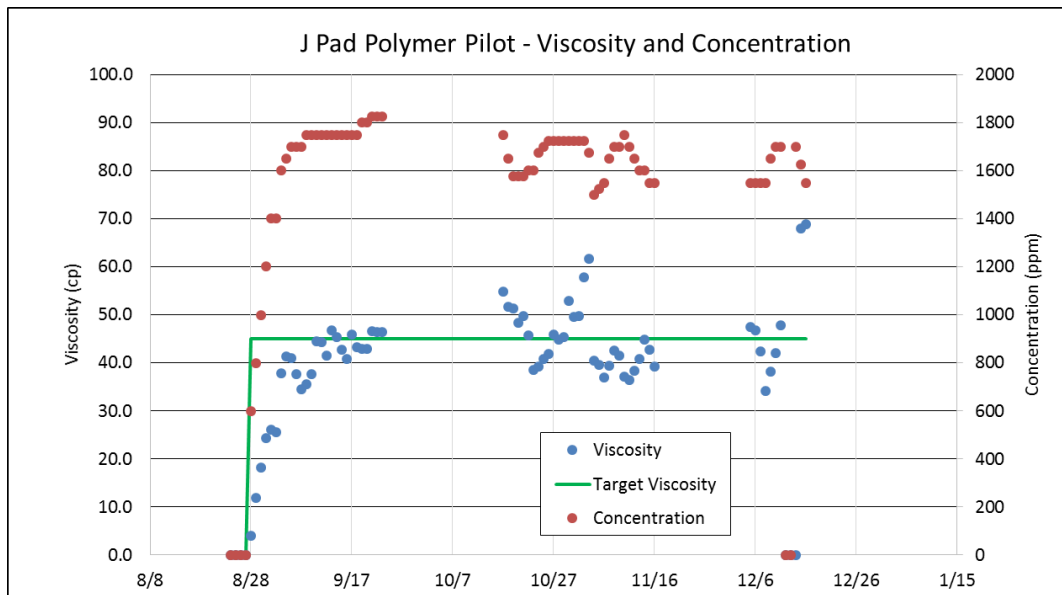
Figure 34 Polymer concentration and viscosity vs. time.

Figure 35 and 36 show daily injection rate and pressure for J-23A and J-24A respectively.
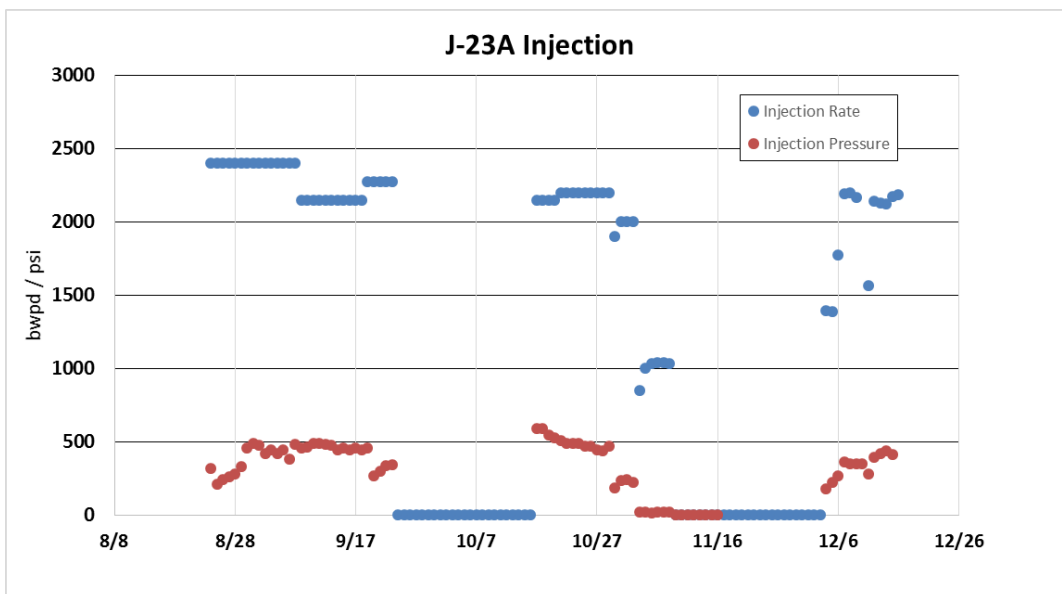
Figure 35 J-23A injection rate and pressure.

44
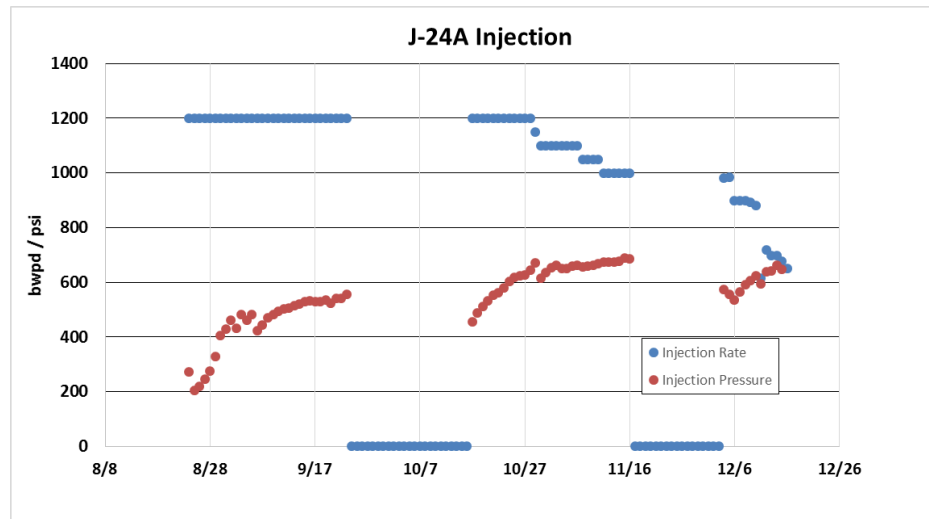
Figure 36 J-24A injection rate and pressure.

Figure 37 is a Hall Plot for both J-23A and J-24A which indicates that the injectivity of J-23A stayed constant (straight line) till a cumulative of 100 mbbl of polymer was injected, then started to increase as evidenced by the decreasing slope. The slope of the Hall Plot for J-24 has been increasing since the polymer startup which indicates that the injectivity of J-24A has been decreasing.
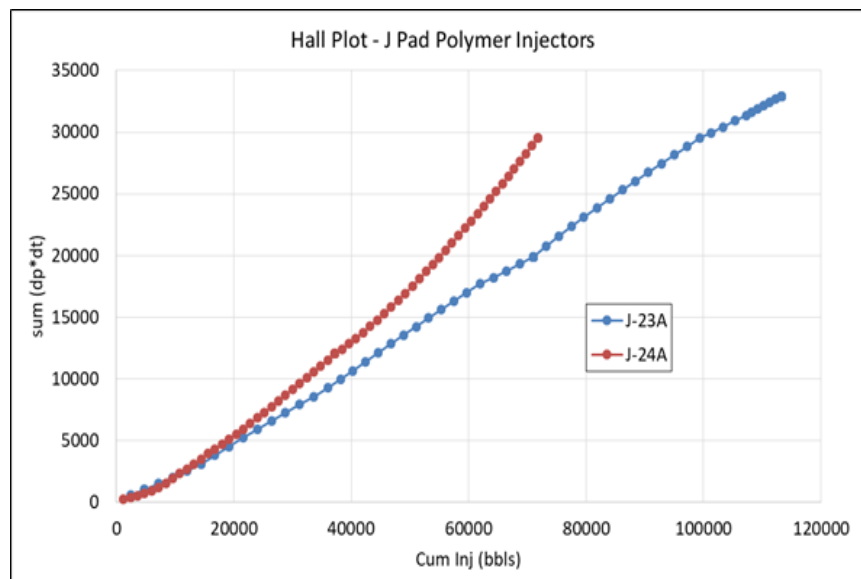
Figure 37 Hall plot for J-23A and J-24A.

University of Alaska Fairbanks

Production performance

Figure 38 depicts the production performance of producer J-27 which is supported by both injectors, J-23A from the south side and J-24A from the North. Oil rate was stable at approximately 900 bpd before polymer injection started on August 28ᵗʰ and increased to about 1200 bpd by end of November. Note that the drastically higher oil rate from mid-October to early November was deemed to be caused by test errors rather than polymer injection. The erroneous test results were noticed in early November and since then the test meter has been re-calibrated. Water cut was approximately 65% before polymer started and decreased to about 50% by end of November.
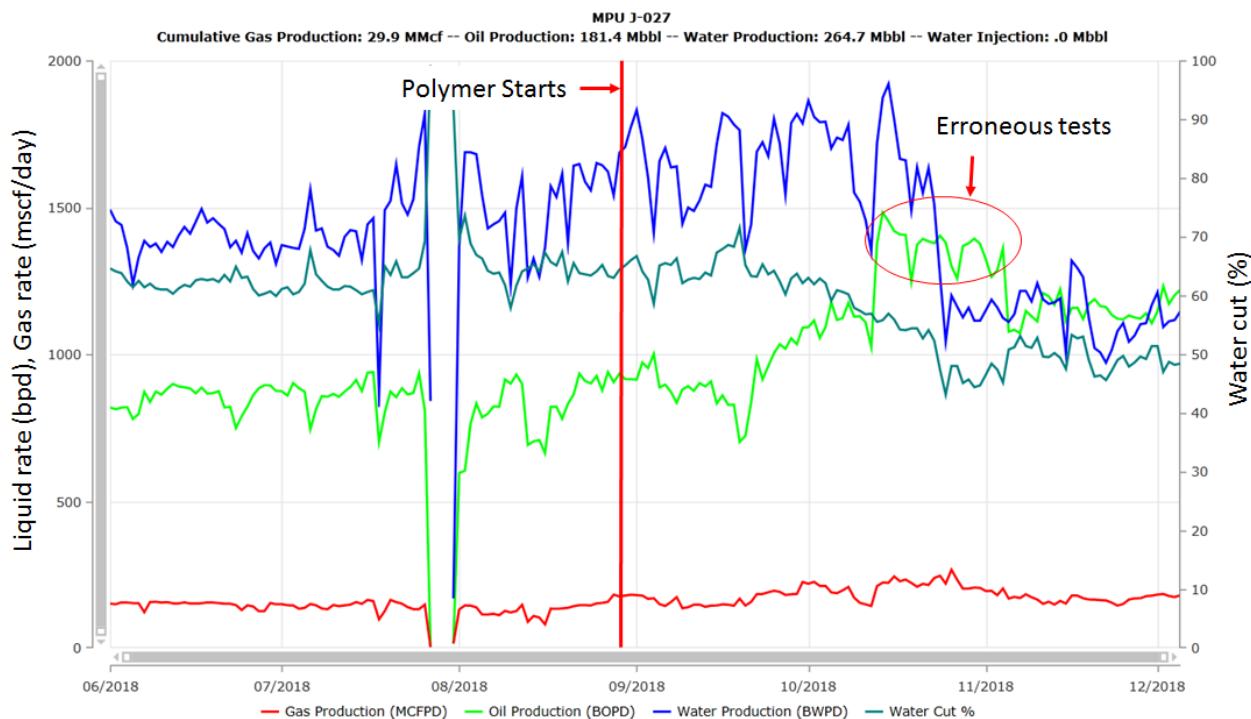
Figure 38 J-27 production performance.

Figure 39 depicts the production performance of producer J-28 which is supported only by injector J-23A from the north side. The horizontal producer was drilled close to a sealing fault to the south side. Oil rate was stable at approximately 500 bpd before polymer started on August 28ᵗʰ and increased to about 630 bpd by end of November while water cut decreased from approximately 70% to about 45% during the same period. The jump in oil rate immediately after polymer startup was most likely due to test errors rather than response to polymer injection.

46
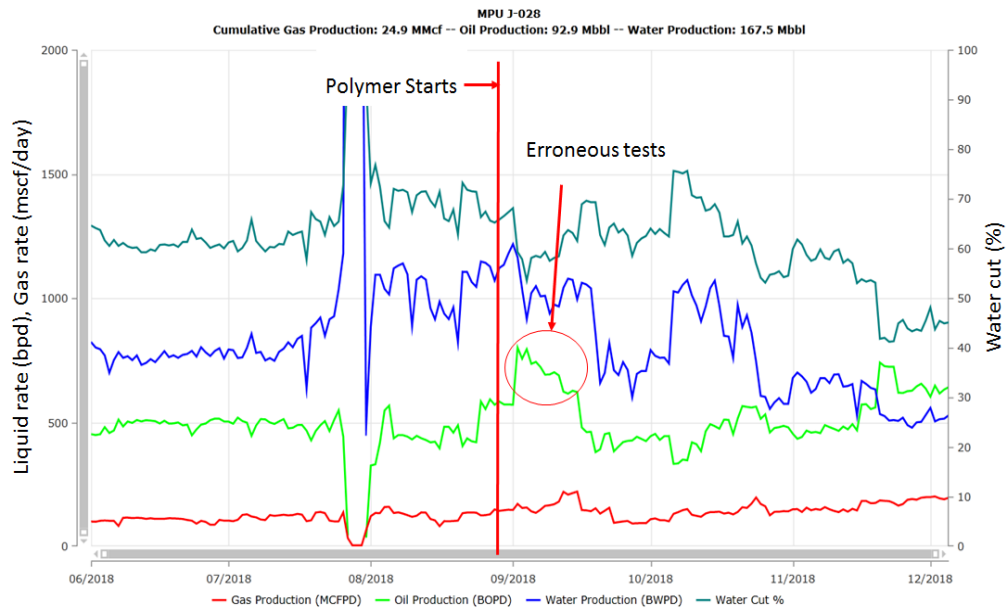
Figure 39 J-28 production performance.

Pre-polymer step rate tests

To assess the wells' water injectivity, downhole gauges were run into injectors J-23A and J-24A on August 12 to perform step rate and PFO tests. **Figure 40** depicts the pre-polymer step rate test of J-23A.
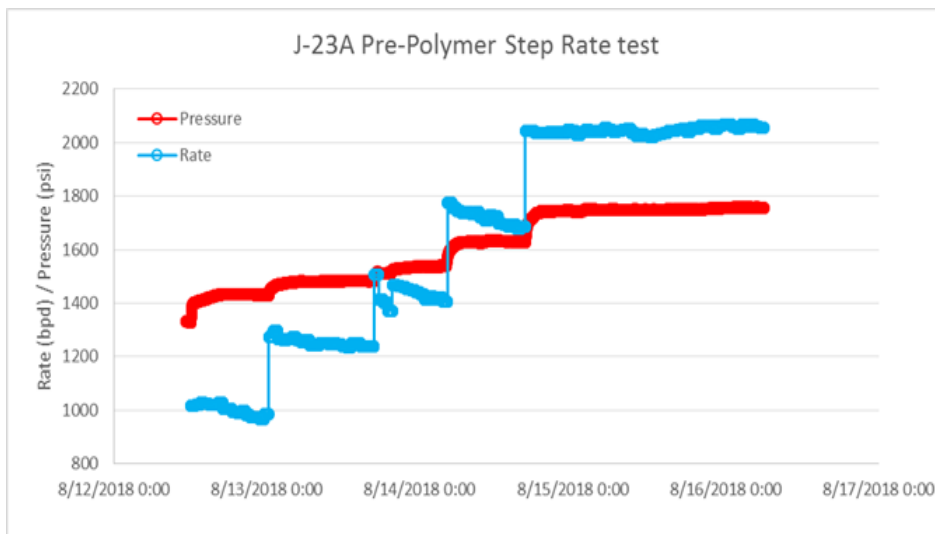
Figure 40 J-23A Pre-polymer step rate test.

47

Figure 41 shows that the bottomhole pressure (BHP) versus water injection rate forms a straight line indicating that the formation was not fractured during water injection. The inverse of the slope of the straight line defines the injectivity index which is estimated to be 3.24 bpd/psi for J-23A for water injection.
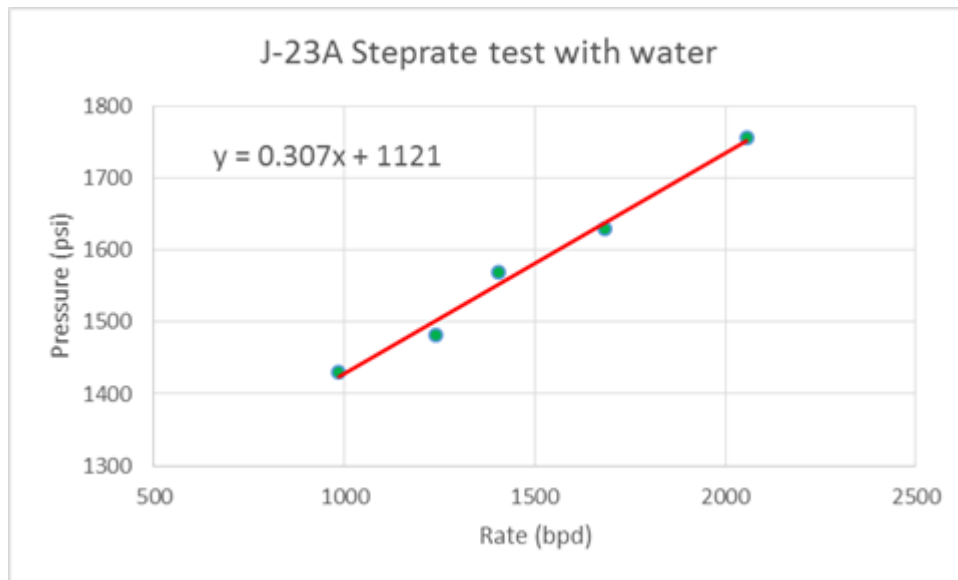
Figure 41 J-23A Pre-polymer step rate test results.

Figure 42 depicts the pre-polymer step rate test of J-24A and **Figure 43** shows the bottomhole pressure (BHP) versus water injection rate relationship.
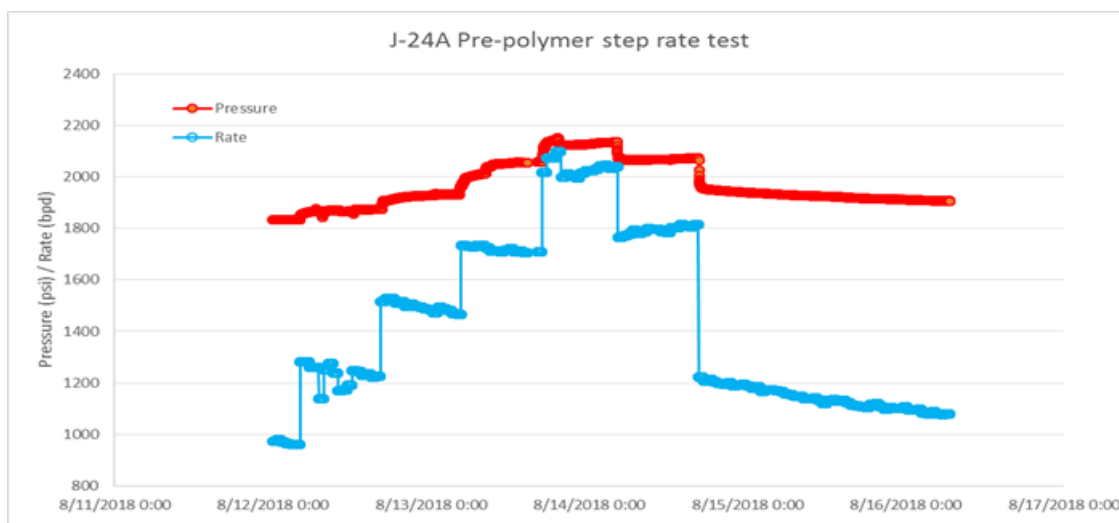
Figure 42 J-24A Pre-polymer step rate test.

Figure 43 shows that the bottomhole pressure (BHP) versus water injection rate forms a straight line

indicating that the formation was not fractured during water injection. The inverse of the slope of the straight line defines the injectivity index which is estimated to be 3.26 bpd/psi for J-24A for water injection.
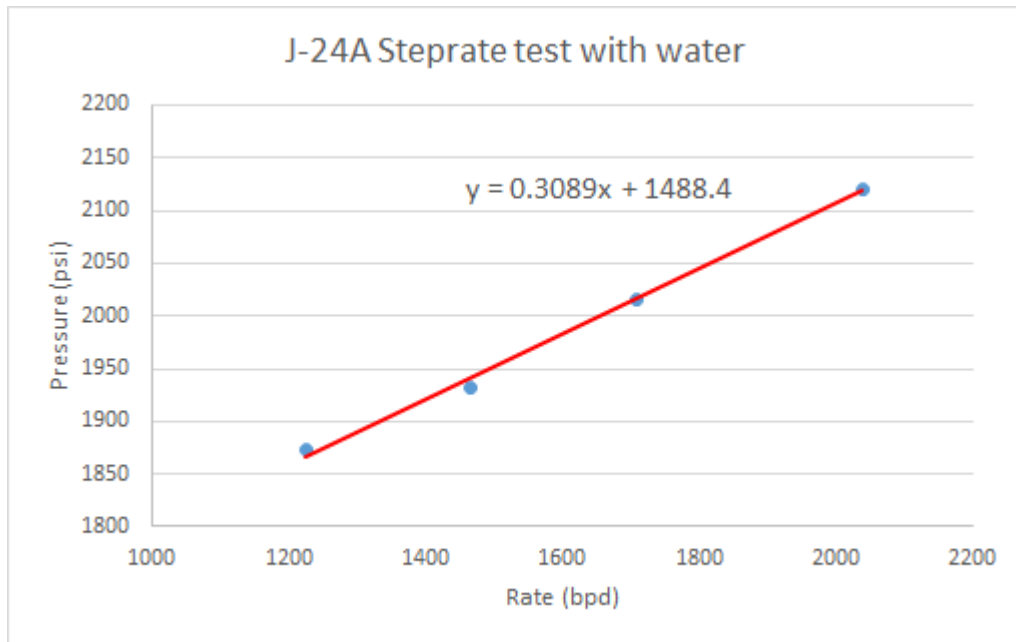
Figure 43 J-24A Step rate test results.

Post-polymer step rate tests

On October 5th, downhole gauges were run again into the two injectors to perform post-polymer step rate and PFO tests. **Figure 44** shows the results of J-23A post-polymer step rate test. The data show a nice linear relationship between the injection pressure and injection rate indicating that the formation was not fractured at the time. The injectivity with polymer is estimated to be 2.9 bpd/psi compared with 3.2 bpd/psi with water. Polymer injectivity only decreased by 10% from water injectivity although the viscosity of the polymer was 45 times higher than that of water, which indicates that injectivity was dominated by oil viscosity rather than water viscosity at the time.
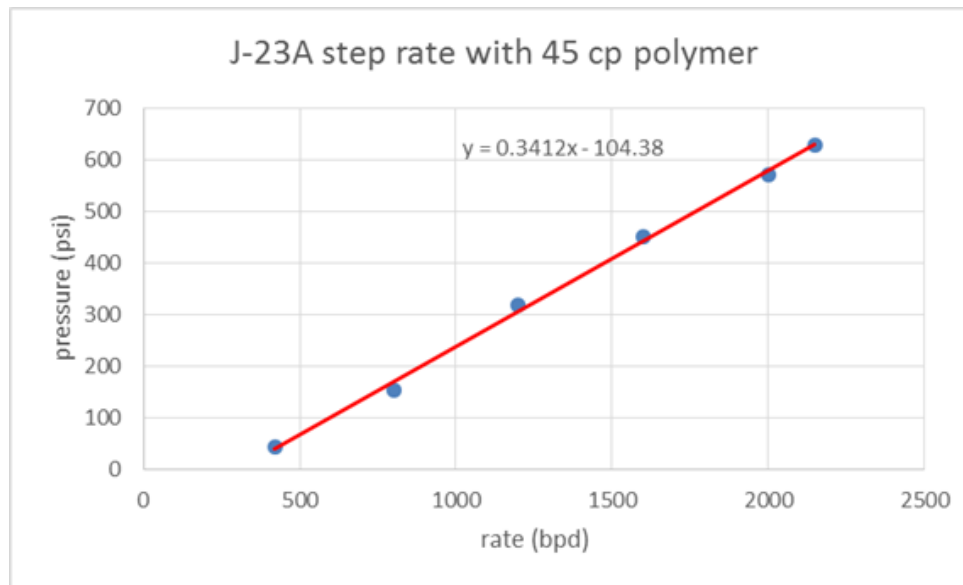
Figure 44 Results of J-23A post-polymer step rate test.

Figure 45 shows the results of J-24A post-polymer step rate test. Again, the data show a nice linear relationship between the injection pressure and injection rate indicating that the formation was not fractured at the time. The injectivity with polymer is estimated to be 4.3 bpd/psi compared with 3.3 bpd/psi with water. This apparent increase was most likely due to the transient effect since the post polymer step rate test was conducted immediately after a 24 day shut in during which reservoir pressure declined due to the ongoing production.
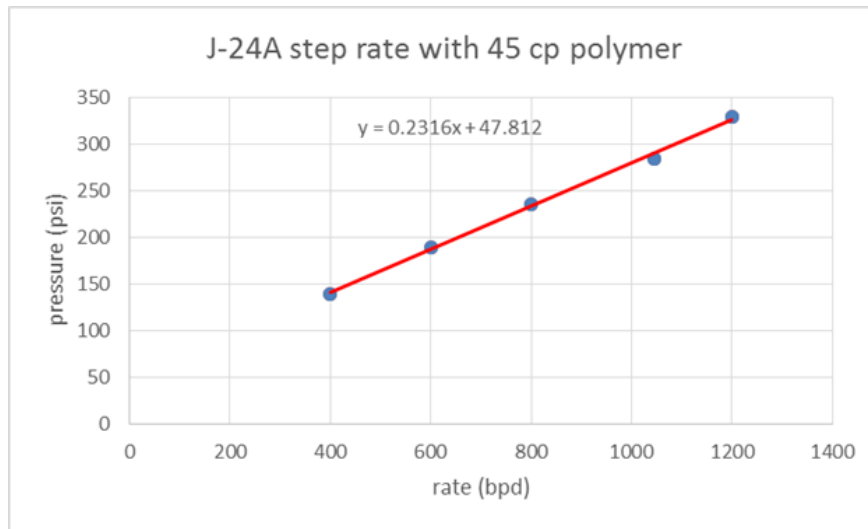
Figure 45 Results of J-24A post-polymer step rate test.

Pressure falloff tests

Pressure falloff (PFO) tests were performed in both injectors, J-23A and J-24A, prior to and after polymer injection started. **Figure 46** is a diagnostic plot of the J-23A pre-polymer PFO test which clearly shows early time radial flow and linear flow regimes as expected in a horizontal well.
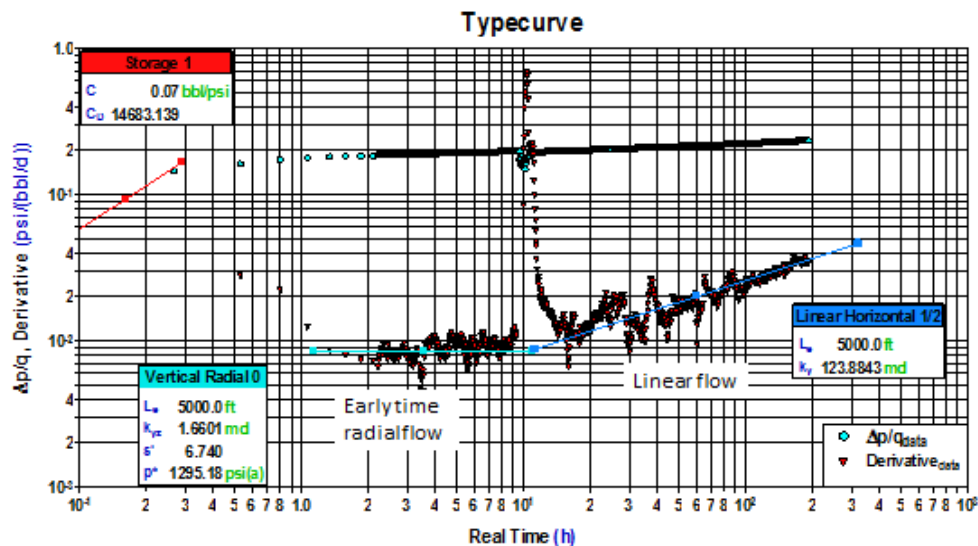
Figure 46 Diagnostic plot of J-23A pre-polymer PFO test.

Figure 47 is a diagnostic plot of the J-23A post-polymer PFO test which shows early time radial flow and late time pseudo radial flow regimes, but the expected linear flow regime was not apparent. This change in flow regimes might have been caused by a change in injection profile along the wellbore. Further analysis indicated that a relatively short section of the 5000 ft wellbore was taking polymer injection in J-23A which is pending on confirmation by an injection profile survey early in 2019. The drop in pressure derivative at late times was most likely caused by the effect of ongoing production from producers, J-27 on the north side and J-28 on the south side.
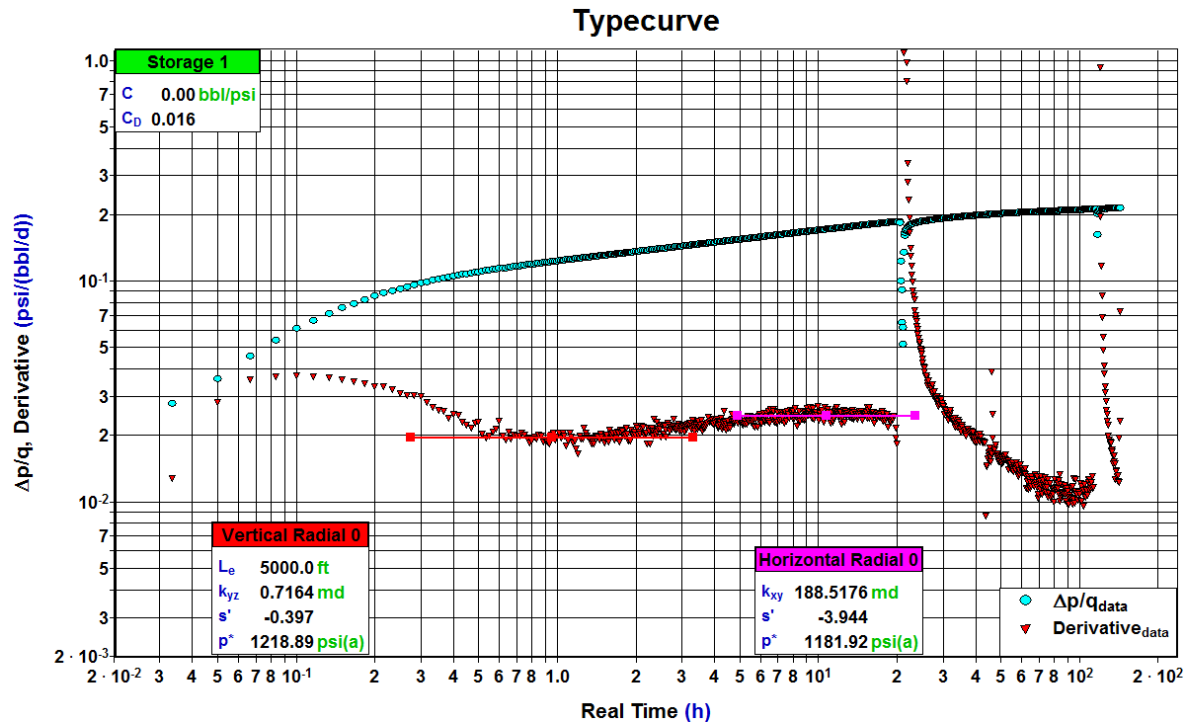
Figure 47 Diagnostic plot of J-23A post-polymer PFO test.

Figure 48 is an overlay of the pressure derivative plots of J-23A pre and post-polymer PFO tests. The plot indicates that the mobility of the injected fluid decreased by 2.5 times near wellbore due to higher viscosity of polymer although the polymer viscosity is 45 times higher than water.
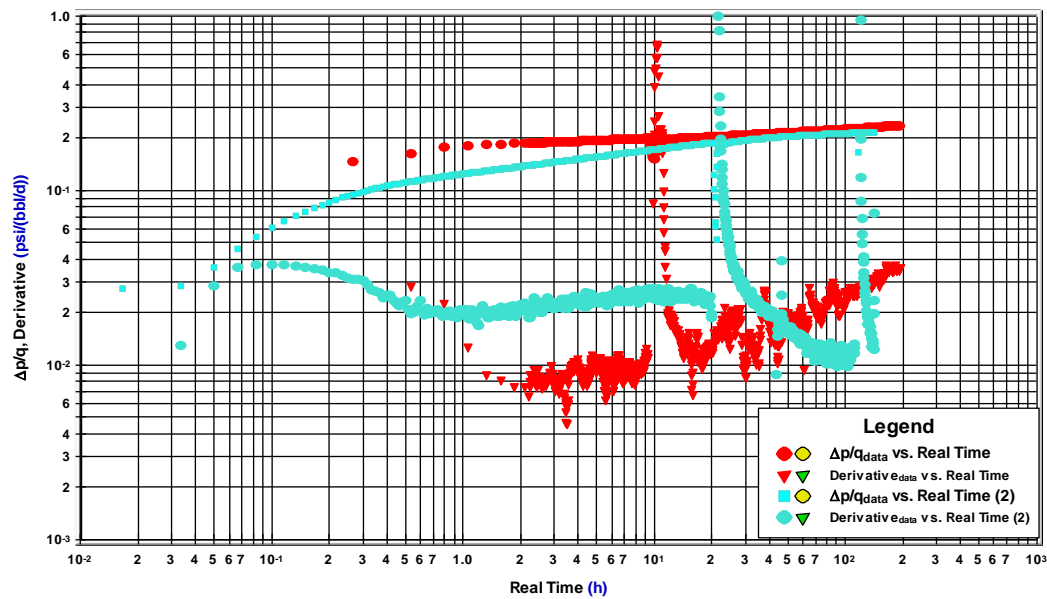
Figure 48 Comparison of J-23A pre and post-polymer PFO tests.

Figure 49 is a diagnostic plot of the J-24A pre-polymer PFO test which clearly shows early time radial flow and linear flow regimes as expected in a horizontal well.
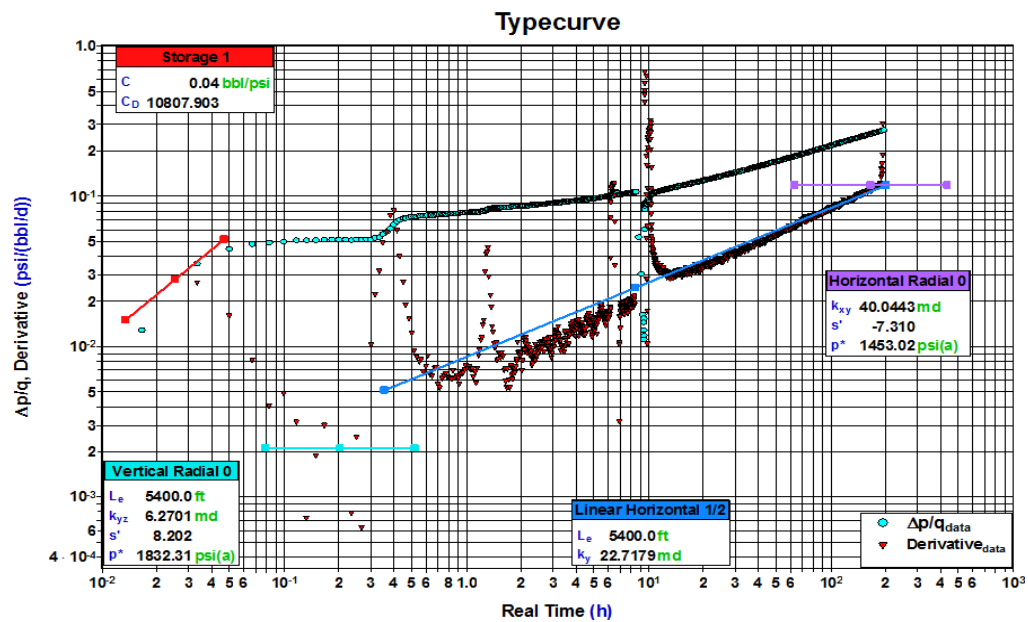
Figure 49 Diagnostic plot of J-24A pre-polymer PFO test.

Figure 50 is a diagnostic plot of the J-24A post-polymer PFO test which also shows early time radial flow and linear flow regimes as expected in a horizontal well.
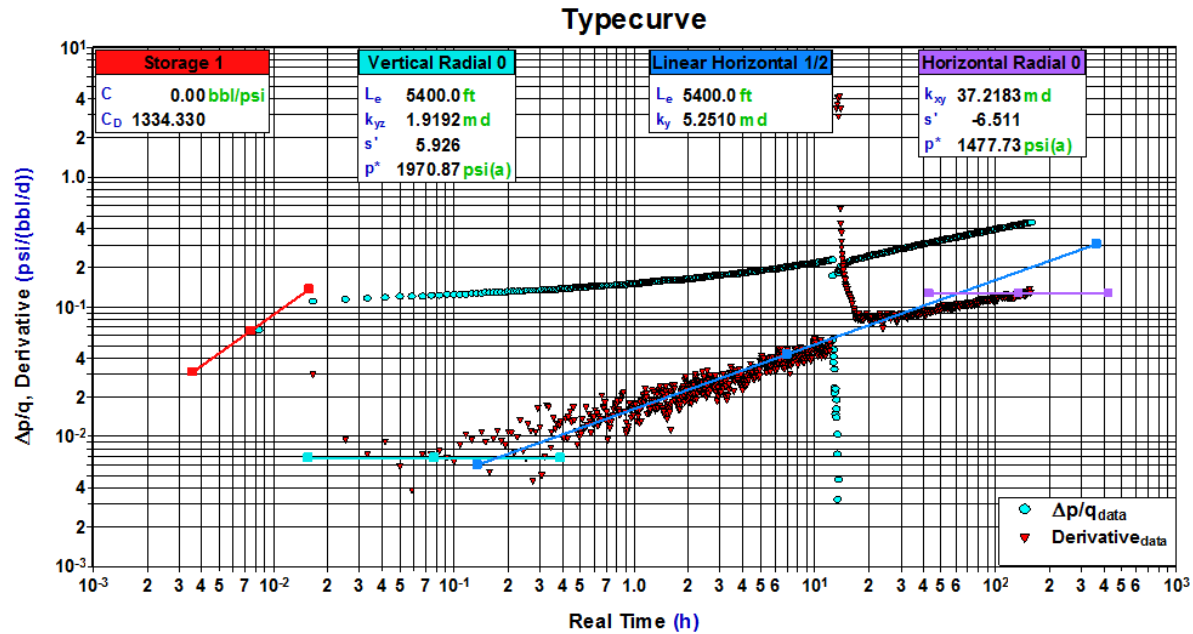
Figure 50 Diagnostic plot of J-24A post-polymer PFO test.

Figure 51 shows the comparison between the pre and post-polymer PFO tests for J-24A. The only apparent difference between the two tests is that the near wellbore mobility of the injected polymer is about 2.5 times lower that of water. Note that the polymer injectivity significantly decreased between the step rate test on October 17th and the PFO on November 16th, 2018. This could be partially due to the transient effect and partially due to the propagation of polymer into the reservoir.
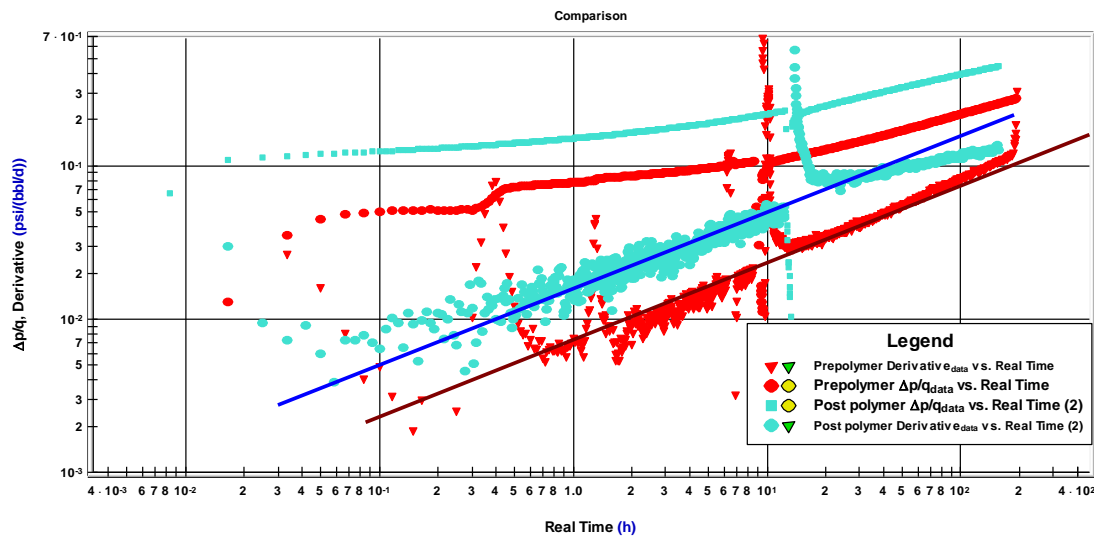
Figure 51 Comparison of J-24A pre and post-polymer PFO tests.

Pre-polymer tracer test

Tracerco's T-140C and T-140A tracers were pumped into injectors J-23A and J-24A respectively on August 3, 2018, 25 days prior to polymer startup to evaluate the breakthrough timing of the injected water. Produced water samples were taken weekly from producers J-27 and J-28 and analyzed in Tracerco's laboratory. Tracer T-140C was first observed in J-27 on October 12, 70 days after injection indicating that water breakthrough from injector J-23A to producer J-27 was happening first. Tracer concentration has been increasing since then as shown in **Figure 52**, but the peak value has not been observed yet which would define the actual water breakthrough timing. No tracers have been detected in producer J-28 as of the date of this writing.
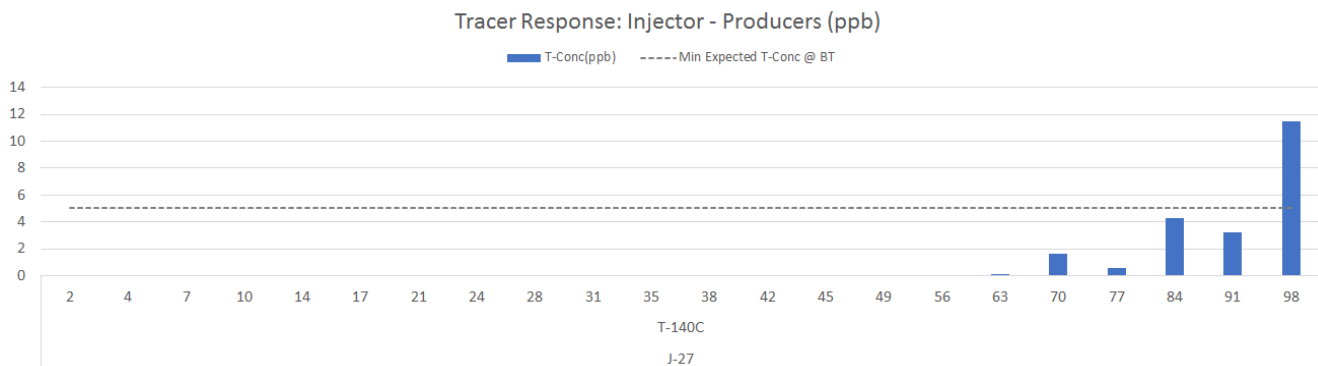
Figure 52 Tracer response from J-23A to J-27.

Activity is ongoing.

● Task 6.0 -Analysis of Effective Ways to Treat Produced Water that Contains Polymer

The formation of stable emulsions during polymer flooding poses significant challenges during oil/water separation in surface production facilities. An efficient way of separating produced crude oil and water is necessary to ensure the cost of flow assurance to be at the lowest. Produced oil and water separation is facilitated by a combination of different techniques and maneuvers such as mechanical, electrical, thermal, and chemical methods, and the introduction of chemical-based additives, i.e., the emulsion breaker, is by far the most common method that helps the most when it comes to emulsion breaking. The chemicals disrupt the interfacial film and enhance the breaking of the emulsion. Earlier studies have shown the importance of emulsion characteristics on the performance and optimization of oil/water separation (Wang et. al., 1999). Further study was performed to carry out an in-depth analysis of the main physicochemical properties of emulsions and the link to their behavior in the field (Zheng ad Cameron). The main objective of this task is to provide recommendations to optimize oil/water separation in the field. The experiments carried out in this task investigate the influence of various factors (physical, mechanical and chemical) on the stability of heavy oil emulsions, and evaluate the efficacy of emulsion breakers.

Fluid samples and experimental procedure
Two types of crude oil and produced water from Milne Point producers B-28 and L-47 are provided by Hilcorp Alaska. The polymer (Flopaam 3630) is provided by SNF, and emulsion breaker is provided by Baker Hughes. Polymer and emulsion breaker were used as received without further purification. Both B-28 and L-47 oil samples were dehydrated by centrifugation at 12000 rpm for 15 minutes and stored in plastic bottles for use. The produced water was filtered using pressure filter after stirring and heating for 45 minutes to remove suspended oil and solid particles. The measured viscosity of B-28 and L-47 oils are 190 and 499 cP respectively at 130°F, and the densities are 0.9303 and 0.9522 g/cm^3 respectively at ambient temperature.

The experimental procedure developed is as follows.
(1)   Polymer solution preparation – add the polymer to purified produced water and mix using a constant speed mixer for 3 hours so that polymer can be completely dissolved in the water.
(2)   Emulsion preparation – treated crude oil, produced water and/or polymer solution are heated to 130°F, and mixed at 5000 rpm for 5 minutes using the water-oil ratios of 30:70 to 90:10 or polymer concentrations of 100, 250 and 500 ppm respectively.
(3)   Emulsion breaker solution preparation – 0.5 g emulsion breaker is added to 50 mL xylene to prepare 10000 mg/L emulsion breaker solution. The amount of solution added into the crude oil emulsion is determined by the total volume of crude oil emulsion to make sure the concentration of emulsion breaker is 100 mg/L.
(4)   Emulsion imaging – a small drop of emulsion was immediately transferred by a syringe onto a piece of glass slide after the emulsion preparation. The type of the emulsion was observed with the aid of Olympus X80, under a total magnification of 50.

(5)   Bottle tests – 50 mL emulsion right after preparation was transferred into 50mL colorimetric tube which was kept in the water bath at 130ºF. During the bottle test, the emulsion was observed to witness the expulsion of water from emulsion with respect to time. The bottle test includes a differential test where the emulsion is added with 0.5 mL emulsion breaker (to witness the interaction of emulsion with emulsion breakers and how they react to the exposure). The results of the volume of water expelled from emulsion with respect to time were plotted to observe the performance of the emulsion breaker under various conditions.

Experimental results
The effect of crude oil type

The emulsion prepared by B-28 oil with a water content of 50% was so stable that no water was separated after 24 hours. However, at the same water/oil ratio, the emulsion prepared by L-47 oil was unstable and was separated into two layers immediately after preparation. Microscopic image for both the top layer and the bottom layer was taken to determine the emulsion type. **Figures 53 and 54** show the microscopic images of the stable B-28 and double layer L-47 emulsions.
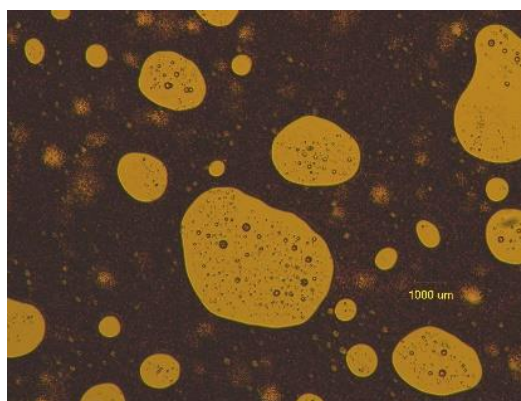
Figure 53 B-28 emulsion with water content of 50% at a magnification of 50 times.
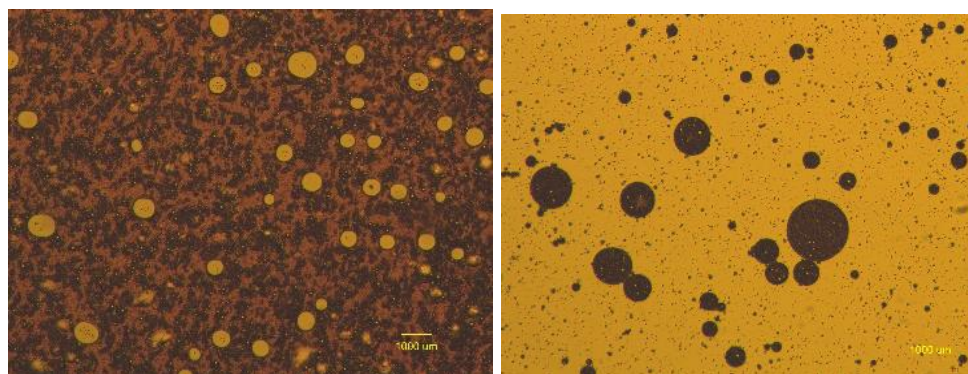
(a) The top layer (water in oil emulsion)   (b) The bottom layer (oil in water emulsion)

Figure 54 L47 emulsion with water content of 50% at a magnification of 50 times.

Figure 55 shows that about 90% of water was separated within half an hour with the addition of 100 ppm emulsion breaker, and without adding emulsion breaker, there was almost no water separated after 240 minutes. **Figure 56** indicates the separated water quality is good, which is transparent and clean, with the addition of the emulsion breaker.
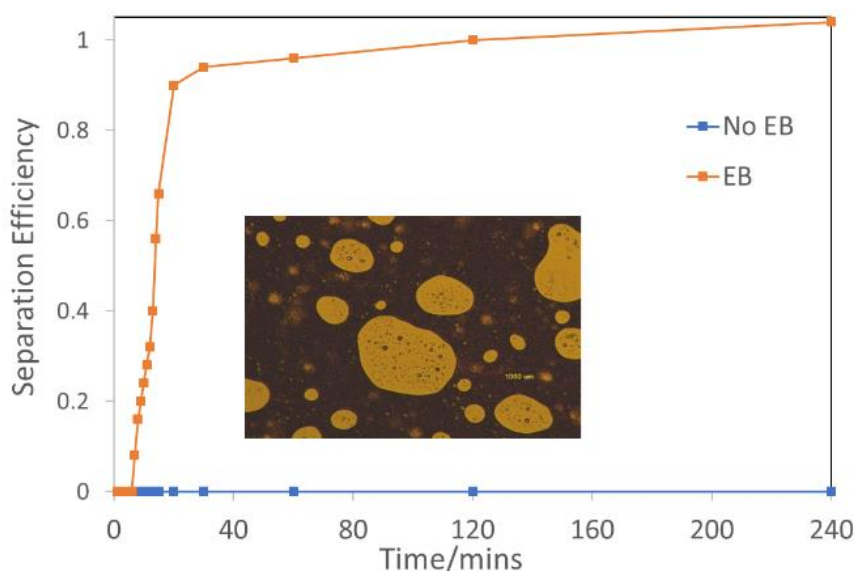
Figure 55 Separation efficiency of B-28 crude oil with respect to time.

(a) 0.25 hr   (b) 0.5 hr   (c) 2 hr   (d) 4 hr
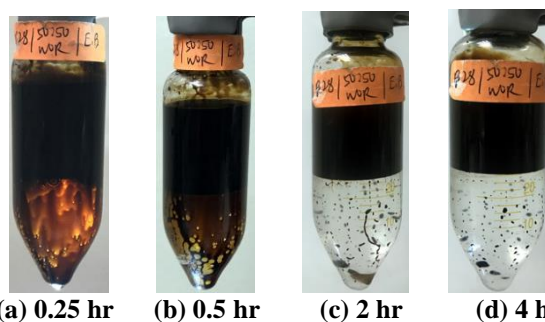
Figure 56 Bottle test of B-28 emulsion with addition of emulsion breaker.

Since the prepared L-47 emulsion is unstable, the water separation efficiency is difficult to determine due to the water content gradient along the tube. The water volume separated from the emulsion is plotted against time to evaluate the performance of the emulsion breaker. As can be seen from **Figure 57**, the separated water volume for emulsion with and without emulsion breaker is similar, indicating the poor stability of the initial emulsion.
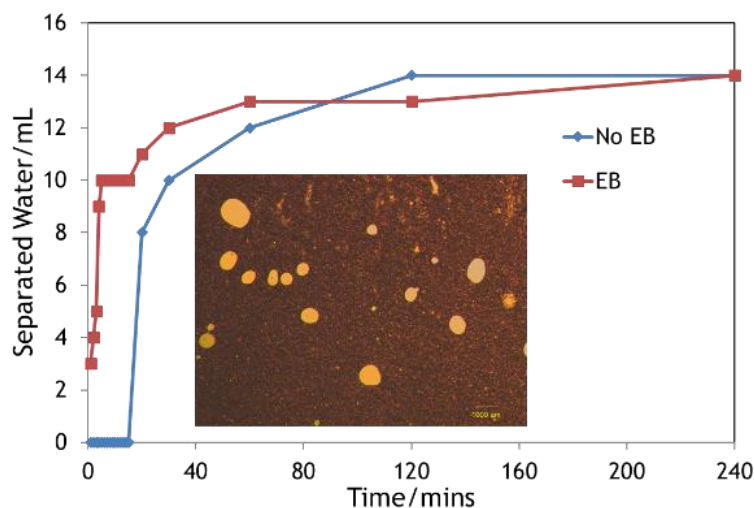
Figure 57 The variation of separated water volume with time.

Comparing the results from **Figures 58 and 59**, the separated water when the emulsion is added with emulsion breaker is much cleaner than that without emulsion breaker.

(a) 0.25 hr   (b) 0.5hr   (c) 2 hr   (d) 4 hr

Figure 58 Bottle test of L-47 emulsion without emulsion breaker.

(a) 0.25 hr   (b) 0.5 hr   (c) 2 hr   (d) 4 hr

Figure 59 Bottle test of L-47 emulsion with emulsion breaker.

In summary, emulsion breaker has a good demulsification efficiency for both B-28 and L-47 emulsions prepared at water/oil ratio of 50:50. The difference between B-28 and L-47 emulsion is the stability at

the initial condition. In other words, B-28 emulsion is much more stable than L-47 emulsion when prepared at the same condition, including the mixing method, emulsion breaker concentration and water/oil ratio.

The effect of water/ oil ratio

Figure 60 shows the microscopic images of B-28 emulsion at various water/oil ratios. As can be seen, at water/oil ratio of 30:70 and 50:50, the emulsion is identified as w/o emulsion, whereas with increasing water content (70% and 90%) the emulsion inverses to complex o/w emulsion. It should be noted that at this turning point where the water/oil ratio reaches 70:30, the stability of o/w emulsion is damaged. The prepared emulsion tends to separate into two layers, among which the top layer is w/o emulsion and the bottom layer is o/w emulsion. Similar to B-28 emulsion, L-47 emulsion turns into o/w emulsion from w/o emulsion when the water/oil ratio is no less than 70:30 (see **Figure 61**).
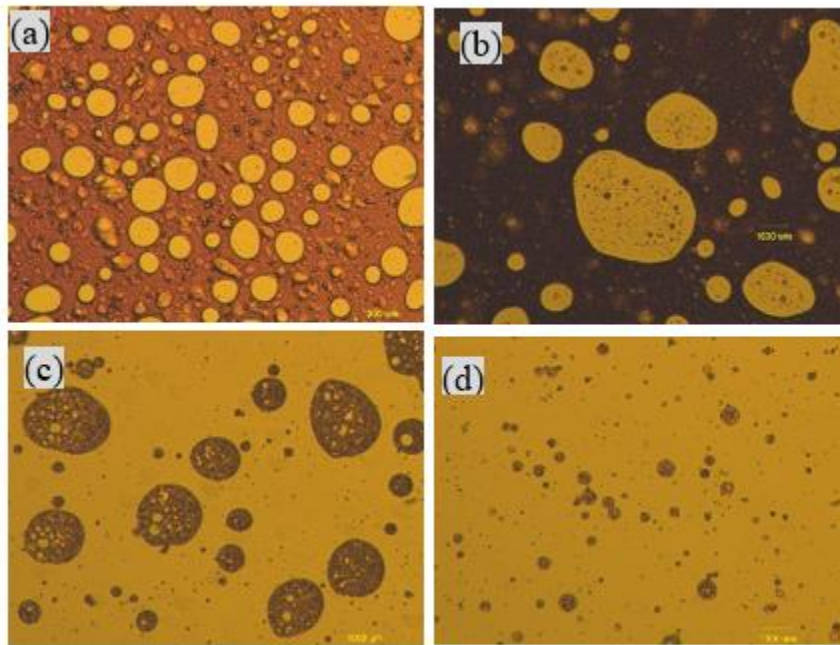
Figure 60 Microscope images for B-28 emulsion at water/oil ratio of (a) 30:70 (b) 50:50 (c) 70:30 (d) 90:10.
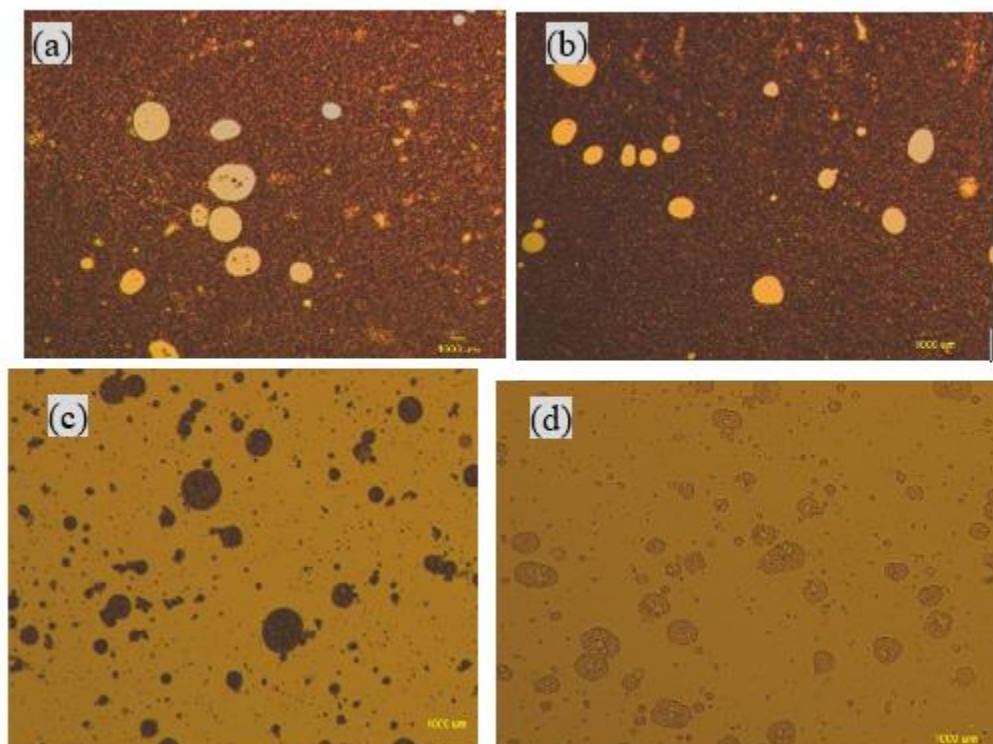
Figure 61 Microscope image for L-47 emulsion at water/oil ratio of (a) 30:70 (b) 50:50 (c) 70:30 (d) 90:10.

Figures 62 – 64 show the water separation and bottle test results for B-28 oil. The separated water volume of crude oil emulsion with (red curve) and without treatment of emulsion breaker (blue curve) as the water content increases from 30% to 90% shows that in the absence of emulsion breaker, the w/o emulsion, formed at the water/oil ratio below 50:50, has a high stability which means no water is separated within 1 hour. When the emulsion breaker is introduced, it exhibits good performance, contributing to a separation efficiency of more than 90%. However, when water/oil ratio is above 70:30, water tends to separate even without addition of emulsion breaker; the difference between the red curve and the blue curve narrows (**Figure 62**). The quality (clarity) of separated water is also observed to evaluate the performance of emulsion breaker at various water/oil ratio. As can be seen from **Figures 63 and 64**, a good water quality is obtained when the emulsion breaker is added into the emulsion with water content less than 50%. Whereas, the effectiveness of the emulsion breaker at water/oil ratio higher than 70% is reduced as indicated by a large amount of residual oil remaining in the separated water phase after 4 hours.

University of Alaska Fairbanks

(a) 30:70

(b) 50:50

(c) 70:30

(d) 90:10

Figure 62 Water separation for B-28 emulsion at water/oil ratio of (a) 30:70 (b) 50:50 (c) 70:30 (d) 90:10

(a) 30:70   (b) 50:50   (c) 70:30   (d) 90:10

Figure 63 Bottle test for B-28 emulsion at water/oil ratio of (a) 30:70 (b) 50:50 (c) 70:30 (d) 90:10 with no emulsion breaker after 4 hours.

(a) 30:70   (b) 50:50   (c) 70:30   (d) 90:10

Figure 64 Bottle test for B-28 emulsion at water/oil ratio of (a) 30:70 (b) 50:50 (c) 70:30 (d) 90:10 with emulsion breaker after 4 hours.

Figures 65 – 67 show the water separation and bottle test results for L-47 oil. At low water content and without emulsion breaker, some amount of water is separated out naturally with poor quality (see **Figure 66(a), (b)**). When adding emulsion breaker, the emulsion breaker accelerates the separation process and improves the separated water quality. For L-47 o/w emulsion at high water content, the emulsion breaker shows a limited and low separation efficiency judging from the cloudy and turbid separated water at the bottom (see **Figure 67(c), (d)**).

(a) 30:70
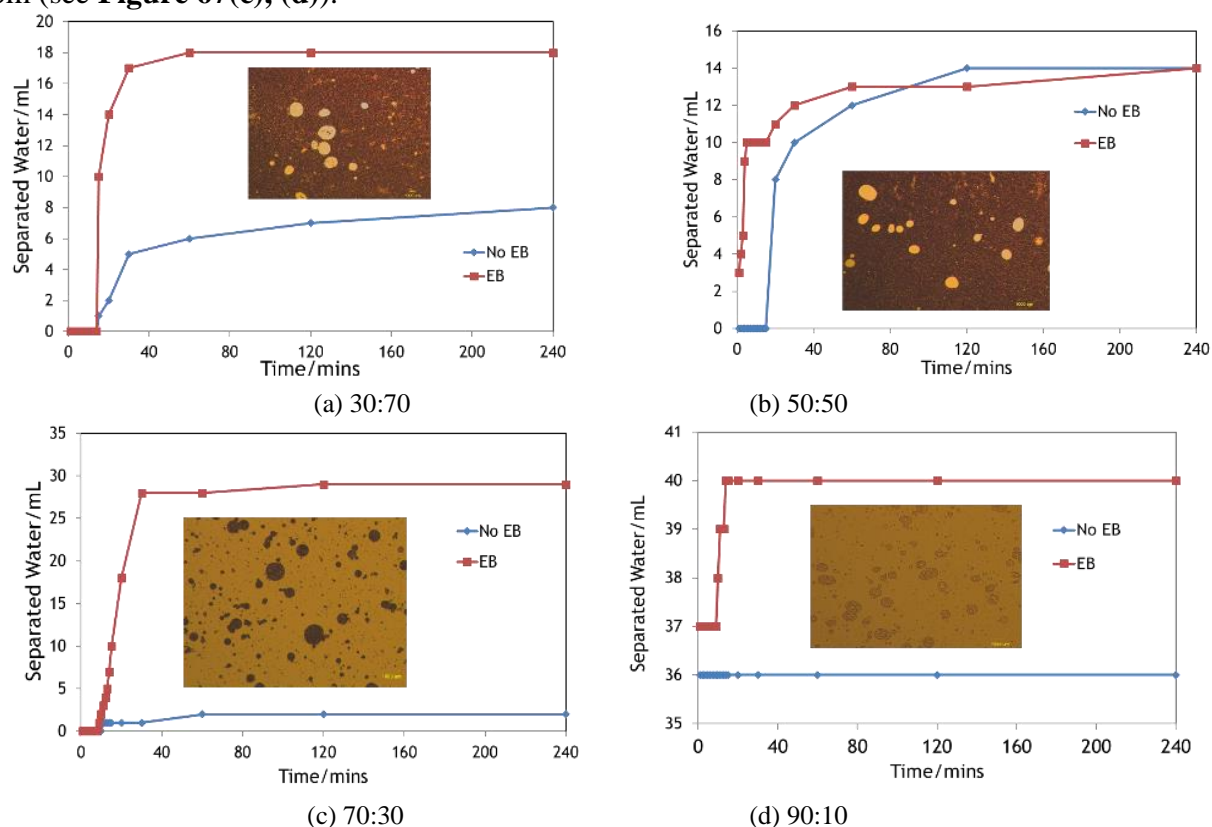
(b) 50:50

(c) 70:30

(d) 90:10

Figure 65 Water separation for L-47 emulsion at water/oil ratio of (a) 30:70 (b) 50:50 (c) 70:30 (d) 90:10.
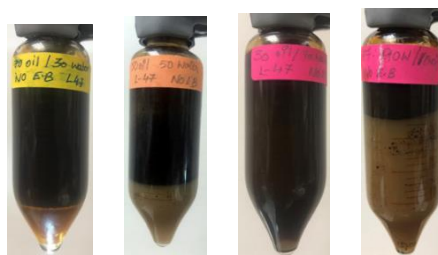
(a) 30:70   (b) 50:50   (c) 70:30   (d) 90:10

Figure 66 Bottle test for L-47 emulsion at water/oil ratio of (a) 30:70 (b) 50:50 (c) 70:30 (d) 90:10 without emulsion breaker after 4 hours.
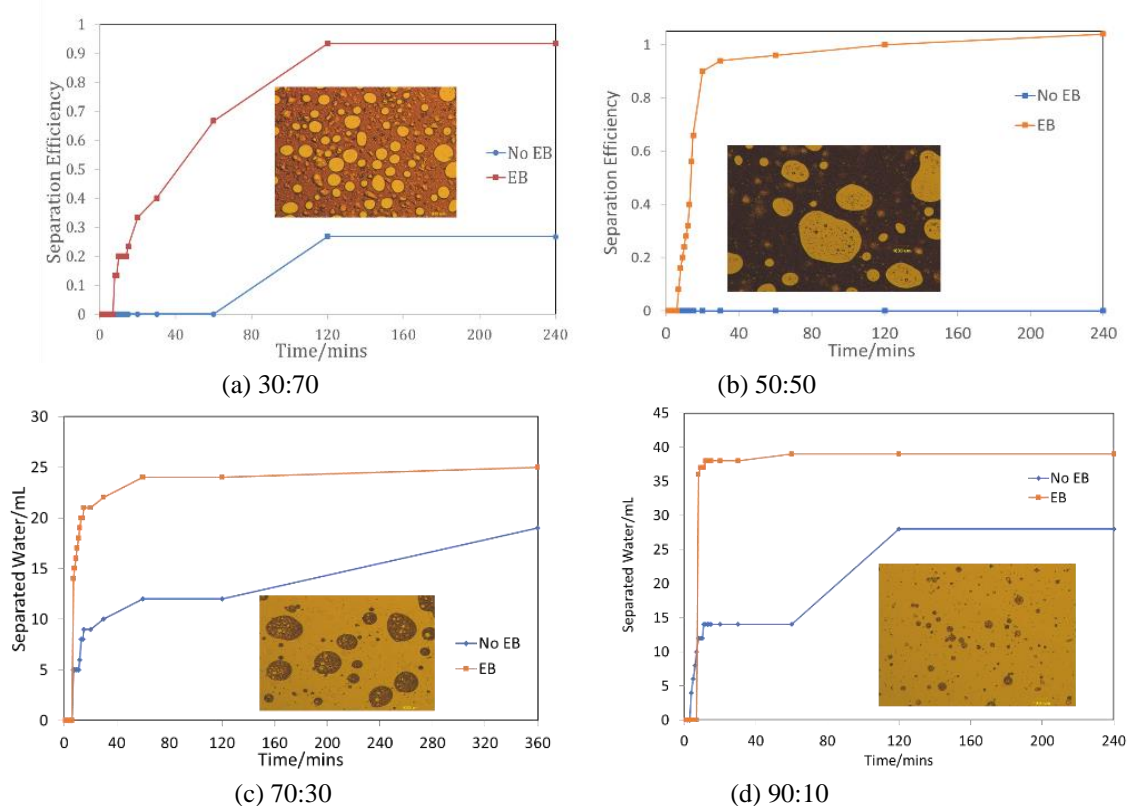

(a) 30:70   (b) 50:50   (c) 70:30   (d) 90:10

Figure 67 Bottle test for L-47 emulsion at water/oil ratio of (a) 30:70 (b) 50:50 (c) 70:30 (d) 90:10 with emulsion breaker after 4 hours.

To summarize, there is a turning point where the emulsion turns into o/w emulsion from w/o emulsion as water/oil ratio increases for both B-28 and L-47 emulsions. After this turning point, the effectiveness of the emulsion breaker significantly reduces.

The effect of polymer concentration

These experiments were carried out with B-28 oil at water/oil ratio of 50:50 at 55°C. The polymer concentration was set at 100 ppm, 250 ppm and 500 ppm. As shown in **Figure 68**, more water droplets are dispersed in the oil phase as polymer concentration increases, which implies that the polymer intensifies the emulsification and increases the difficulty in separating the dispersed droplets.
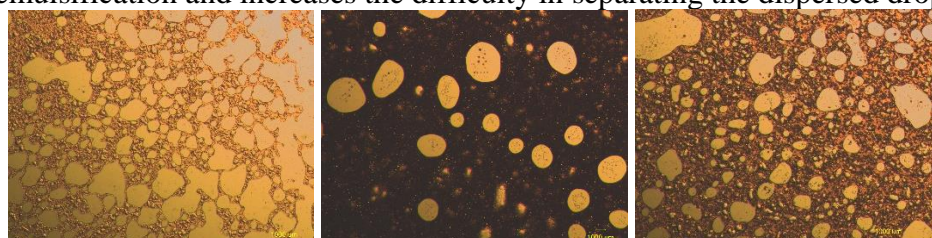
(a) 100ppm   (b) 250ppm   (c) 500ppm

Figure 68 Microscopic image for B-28 emulsion at polymer concentration of (a) 100 ppm (b) 250 ppm (c) 500ppm.

Without emulsion breaker, the effect of polymer on the stability of B-28 emulsion can be identified from **Figure 69** which shows that polymer has a complicated interaction with crude oil. The 100 ppm polymer tends to promote the coalescence of dispersed water droplets, while the 250 ppm polymer appears to enhance the stability of the emulsion. When polymer concentration increases to 500ppm, separation becomes easier again. Obviously as seen in **Figure 70**, the separated water quality is negatively impacted when the polymer is present in the system.
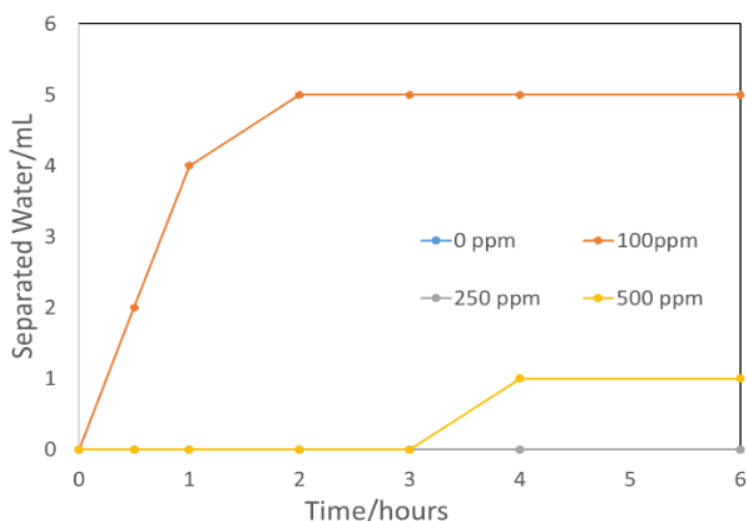
Figure 69 Separated water volume vs. time with various polymer concentration for B-28.
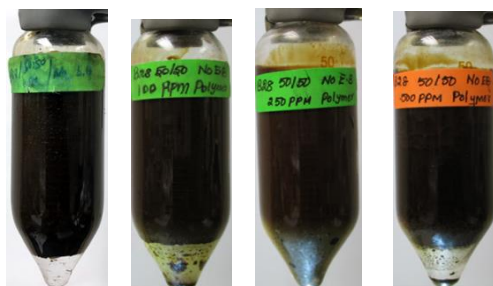
(a) 0 ppm   (b) 100 ppm (c) 250 ppm   (d)500 ppm
Figure 70 Bottle test for B-28 emulsion without emulsion breaker at polymer concentration of (a) 100 ppm (b) 250 ppm (c) 500ppm after 24 hours.

By adding emulsion breaker, the polymer concentration has little effect on the separated water volume and separation rate as shown in **Figure 71**. When the separated water quality is considered (see **Figure 72**), the bottom half of the tube remains somewhat yellow stained indicating the presence of tiny oil droplets remaining in the water phase, especially at a polymer concentration of 100 ppm.
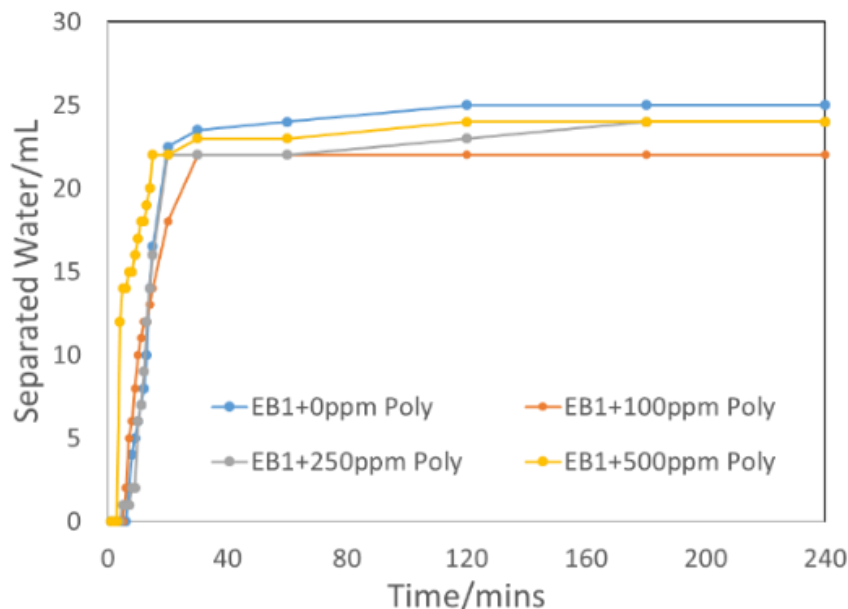
Figure 71 Separated water volume vs. time with emulsion breaker and various polymer concentration.

(a) 0 ppm   (b) 100 ppm   (c) 250 ppm   (d)500 ppm

Figure 72 Bottle test for B-28 emulsion with emulsion breaker at a polymer concentration of (a) 100 ppm (b) 250 ppm (c) 500ppm after 24 hours.

Overall, for both B-28 and L-47 crude oil emulsions, emulsion breaker has a low demulsification efficiency when the water/oil ratio is greater than 70:30 at which an inverse o/w emulsion occurs, and there is a reduction in the efficiency of the emulsion breaker when polymer is present. For L-47 oil, surprisingly it cannot form stable emulsion even at low water content, which may be a result of chemical additives in the crude oil sample. Future work is focusing on repeating some tests with different oil and water samples, especially considering the effect of polymer on emulsion breaker efficiency, studying new emulsion breakers, and measuring the oil content in the separated water.

Activity is ongoing.

● Task 7.0 - Feasibility of Commercial Application of the Proposed Advanced Polymer Flooding in

University of Alaska Fairbanks

ANS Heavy Oil Reservoirs

Activity has not yet started.

c. Opportunities for Training and Professional Development

All the graduate students working on the project are obvious recipients of training and professional development in petroleum engineering.

d. Dissemination of Results to Communities of Interest

The PI of the project volunteered to deliver a public seminar in the College of Engineering and Mines as part of the SPE student chapter at UAF to basically educate the general engineering community as far as this project is concerned. This event took place on October 19th and the current plan is to deliver frequent seminars on the project as updates, because this is of particular importance to the citizens of State of Alaska with 80+% of its economy based on the oil industry.

e. Plan for Next Quarter

Building on the current progress achieved by the research team, work planned for the next quarter will include steadily progressing toward the planned completion dates outlined in **Table 8** below.

Table 8 Summary of milestone status.

Milestones	Task No.	Planned Completion Date	Actual Completion Date	Verification Method	Comments
Project Management Plan	1a	o 9/30/2022	o Ongoing	Report	None
Data Management Plan	1b	o 8/31/2018	o 7/20/2022	Report	None
● Quantify polymer retention	2	o 3/31/2019	o Ongoing	Report	None
● Effect of water salinity on S_{or} ● Screening of gel products for conformance control	3	o 4/30/2019 o 6/30/2019	o Ongoing o Initiated	Report	None

● Pilot area model waterflooding history match ● Coreflooding model history match ● Updated area model for polymer flood prediction ● Reservoir modeling report	4	o 12/312018 o 4/30/2019 o 5/31/2019 o 5/31/2019	o Ongoing o Ongoing o Initiated o Not yet started	Report	None
● Injection profile with polymer inj. ● PFO (post-polymer) ● Tracer tests (post-polymer)	5	o 12/31/2018 o 12/31/2018 o 12/31/2018	o Ongoing o Ongoing o Ongoing	Report	None
● Initial treatment plan recommendation based upon literature survey	6	o 12/31/2018	o Ongoing	Report	None

2. PRODUCTS

Following is the citation of the abstract that has been accepted. As soon as the conference technical program committee finalizes the program it will appear on the SPE website.

A.Y. Dandekar, University of Alaska - Fairbanks; B. Bai, Missouri University of Science & Tech; J.A. Barnes, Hilcorp Alaska LLC; D.P. Cercone, J. Ciferno, National Energy Technology Laboratory; S.X. Ning, Reservoir Experts LLC; R.S. Seright, New Mexico Inst-Mining & Tech; B. Sheets, University of Alaska Fairbanks; D. Wang, University of North Dakota; Y. Zhang, University of Alaska – Fairbanks: "First Ever Polymer Flood Field Pilot - A Game Changer to Enhance the Recovery of Heavy Oils on Alaska's North Slope". Selected for presentation at the SPE Western Regional Meeting to be held 23-26 April 2019 in San Jose, California, USA. SPE-195257-MS. Note – the manuscript for this accepted paper is due in February 2019.

3. PARTICIPANTS & OTHER COLLABORATING ORGANIZATIONS

Hilcorp hired two operators dedicated to the project operations. Two reservoir engineers are in charge of the test design and analysis; one facilities engineer is in charge of polymer skid design and installation; and one operations engineer is in charge of downhole well work.

All the listed project personnel identified on the second page, the post-doc, and graduate students working on different tasks formally contribute 2 hours every other Friday in a project working meeting. Additionally, sub-group working meetings, typically lasting for 2-4 hours in a month are also held to discuss specific tasks such as reservoir simulation. For the post-doc and graduate students the typical formal working hours per week are 40 and 20 respectively, whereas the latter is typical of personnel identified in the aforementioned table to supervise the students. Besides these, additional hours are typical in preparing reports, presentations for meetings, and potential publications.

4. IMPACT

The project PI has actually showcased the project in an undergraduate class on reservoir rock and fluid properties (PETE301), in relevant lecture topics such as mobility ratio, relative permeability, displacement efficiency and residual oil saturation. This will continue in the future offerings as well as other relevant classes in the petroleum engineering curriculum. So far this has had a positive impact in that the students can easily relate the theory to what is being implemented in practice in the field. Finally, this also has a relevant impact from the accreditation standpoint which requires continuous improvement of different elements of the program.

5. CHANGES/PROBLEMS

a) The PSU has been modified and reclassified as Class I Division II facility to accommodate the presence of hydrocarbon gas in the source water used to make polymer solution;
b) Injection pumps, P-6000 and P-8000, broke down in the first 3 months but have been repaired;
c) Errors occurred in field test data, portable separator was brought in to verify rates;
d) Team recognized a new challenge with regard to the deposition of polymer, mineral scale and

their mutual interaction in heater tubes which need be investigated with expanded scope;
e) Produced water and polymer foams when mixed and the presence of polymer impairs the demulsification efficiency.

6. **SPECIAL REPORTING REQUIREMENTS**
   Nothing to Report.

7. **BUDGETARY INFORMATION**
   A summary of the budgetary information for the first budget period of the project is provided in **Table 9**. This table shows the planned costs, reported costs, and the variance between the two. Reported costs is the sum of UAF's incurred expenses and the sum of the invoices received from our project partners.

Table 9 Budgetary information for Budget Period 1, Q2.

Baseline Reporting Quarter	Budget Period 1	
	September-November 2018	
	Q2	Cumulative Total
Baseline Cost Plan		
Federal Share	$1,121,947	$1,625,996
Non-Federal Share	$146,696	$670,564
Total Planned	**$1,268,643**	**$2,296,561**
Actual Incurred Cost		
Federal Share	$878,129	$962,965
Non-Federal Share	$542,595	$542,595
Total Incurred Cost	**$1,420,724**	**$1,505,560**
Variance		
Federal Share	-$243,818	-$663,032
Non-Federal Share	+$395,900	-$127,969
Total Variance	**+152,082**	**-$791,001**

Please note that the PMP also has a spending plan that is based on calendar quarters.

8. PROJECT OUTCOMES
Nothing to Report.

9. REFERENCES

Austad T, 2008, 'Smart Water' for Enhanced Oil Recovery: A Comparison of Mechanisms in Carbonates and Sandstones, presentation at the FORCE seminar on Low Salinity, NPD, Stavanger.

Austad T et al, 2010, Chemical Mechanism of Low salinity Water Flooding in Sandstone Reservoirs, SPE 129767, SPE IOR Symposium, Tulsa.

Ayirala S, et al, 2010, A Designer Water Process for Offshore Low Salinity and Polymer Flooding Applications, SPE 129926, SPE IOR Symposium, Tulsa.

Buckley J, 2009, Low Salinity Waterflooding - An Overview of Likely Mechanisms, on-line presentation.

Heigre E, 2008, Low Salinity Water Injection - Heidrun Field Case Study, presentation at the FORCE seminar on Low Salinity, NPD, Stavanger.

Hughes DS, 2003, Presentation on Modelling of Possible Hydragel Wettability Effect, part of a study Mechanistic Investigation of a Novel Polymer/Surfactant and Identification/Design of Potential Field Trial, A02DTI09, RML for DTI, 2004.

Jerauld GR et al, 2006, Modelling Low-Salinity Waterflooding. SPE 102239 Kehew AE, 2001, The Geochemistry of Natural Waters (Chapter 4).

Lager A et al, 2006-8, BP Low Salinity Patent Application (Hydrocarbon Recovery Process), PCT/GB2007/003337 - WO 2008/029124 A1.

Lager A et al, 2006, Low Salinity Oil Recovery – An Experimental Investigation, SCA2006-36, presented at the Society of Core analysts meeting, Trondheim.

Lager A et al, 2007, Impact of Brine Chemistry on Oil Recovery, presented at the 14th EAGE European Symposium on EOR, Cairo.

Lake LW, 1989, Enhanced Oil Recovery, Prentice-Hall.

Lee SY et al, 2010, Low Salinity Oil Recovery - Increasing Understanding of the Underlying Mechanisms, SPE 129722, SPE IOR Symposium, Tulsa.

Ligthelm D et al, 2009, Novel Waterflooding Strategy by Manipulation of Injection Brine Composition, SPE 119835, SPE EUROPEC/EAGE Annual Conference and Exhibition held in Amsterdam.
Lower SK, 1996, Solids in Contact with Natural Waters, text from Simon Fraser University.

Seccombe, Jim, Arnaud Lager, Gary Jerauld, Bharat Jhaveri, Todd Buikema, Sierra Bassler, John Denis, Kevin Webb, Andrew Cockin, and Esther Fueg. "Demonstration of Low-Salinity EOR at Interwell Scale, Endicott Field, Alaska." In SPE Improved Oil Recovery Symposium. 2010.

Tang G and Morrow N, 1999, Oil Recovery by Waterflooding and Imbibition - Invading Brine Cation Valance and Salinity, SCA 9911.

Tang G and Morrow N, 1999b, Influence of Brine Composition and Fines Migration on Crude Oil/Brine/Rock Interactions and Oil Recovery, Proceedings of the 5th International Symposium on Evaluation of Reservoir Wettability and its Effect on Oil Recovery, Trondheim, Norway, June1998, and published in J Pet. Sci. Eng, 24: 99-111.

Vledder P et al, 2010, Low Salinity Water Flooding: Proof of Wettability Alteration on a Field Wide Scale, SPE 129564, SPE IOR Symposium, Tulsa.

Wang Z.Zhao, L.Li,F., He.,J and Chen.L, 1999. Characteristics study of hydrocyclone used for separating polymer flood produced water, International offshore and polar engineering conference, Best, France, May-1999.

Webb K, 2008, The LoSal EOR process: From Laboratory to Field, presentation at the FORCE seminar on Low Salinity, NPD, Stavanger.

Zheng.F, Quiroga.P, Cameron. Challenges in Processing produced emulsion from chemical enhanced oil recovery – polymer flood using polyacrylamide, SPE 144322.